JOURNAL OF PETROLOGY | VOLUME 37 | NUMBER 4 | PAGES 785–810 | 1996

HARRY BECKER*
MAX-PLANCK-INSTITUT FÜR CHEMIE, ABT. GEOCHEMIE, POSTFACH 3060, D-55020 MAINZ, GERMANY

Crustal Trace Element and Isotopic Signatures in Garnet Pyroxenites from Garnet Peridotite Massifs from Lower Austria

Garnet-bearing high-temperature peridotite massifs in lower Austria were exhumed during Carboniferous plate convergence in the Bohemian massif. The peridotite massifs contain garnet pyroxenite layers, most of which are high-pressure cumulates that crystallized in the deep lithosphere during ascent and cooling of hot asthenospheric melts. Many of the pyroxenites have negative Eu anomalies and high LREE abundances in pyroxenes and bulk rocks, $^{87}Sr/^{86}Sr$ (335 Ma) as high as 0·7089, and ε_{Nd} (335 Ma) as low as −4·8 (leached clinopyroxenes and garnets). These pyroxenites also show strong depletions in Rb, K, Ta, P and Ti compared with the REE. Equilibrium melt compositions calculated from the cumulate compositions have very high LREE abundances (La_n = 300–600) and show strong LREE fractionation [$(La/Sm)_n$ = 7–47)]. Trace element abundances, the Ca–Al-rich composition of the cumulates and possible Ti saturation in the melts suggest that these melts were of primitive carbonatitic–melilitic or lamprophyre-like composition. Other garnet pyroxenites such as Al-rich garnet–kyanite clinopyroxenites with positive Eu anomalies probably represent metamorphosed crustal rocks which were subducted and accreted to the lithospheric mantle. The high $^{87}Sr/^{86}Sr$, low ε_{Nd} (335 Ma) and negative Eu anomalies of the high-pressure cumulates can be explained if their equilibrium melts contained a component derived from subducted upper-crustal rocks. The high equilibration pressures of the host peridotites (3–3·5 GPa) and the high equilibration temperatures of the pyroxenites (1100–1400°C) indicate that these melts are likely to be derived from the sub-lithospheric mantle. There, melting may have been triggered by small amounts of melt or fluids derived from a subducting slab at greater depth.

KEY WORDS: *garnet pyroxenites; geochemistry; lower Austria; ultramafic massifs; subduction*

INTRODUCTION

Pyroxenites found as layers in ultramafic massifs and in mantle xenoliths are physical manifestations of chemical heterogeneities in the upper mantle. Mantle pyroxenites have been interpreted as cumulates that formed by partial freezing of melts in the upper mantle (e.g. Green & Ringwood, 1967; Kornprobst, 1969). Such a partial freezing may occur in the lithosphere as a result of temperature differences between ascending melts and their peridotitic wallrock. Another major process that could explain the presence of pyroxenites in mantle peridotites is recycling of subducted oceanic lithosphere into the convecting mantle. It has been suggested that pyroxenites may represent remnants of the basaltic layer of subducted lithosphere, which has been stretched during entrainment in the convecting mantle (Polvé & Allégre, 1980; Allègre & Turcotte, 1986). Pyroxenites from many ultramafic massifs have trace element and isotopic compositions indicating that they crystallized from melts derived from mantle sources characterized by long-term depletion of incompatible elements (e.g. Polvé & Allegre, 1980; Voshage *et al.*, 1988). Pyroxenites from the large lherzolite massif near Beni Bousera are a remarkable exception in that they show extreme variations in isotopic compositions, encompassing the entire range from depleted mantle-like values to sediment-like compositions (Kornprobst *et al.*, 1990; Pearson *et al.*, 1991, 1993). These compositions have been interpreted to result from the presence of a component of recycled sediment and oceanic crust in the parent melt (Pearson *et al.*, 1993).

* Present address: Department of Terrestrial Magnetism, Carnegie Institution of Washington, 5241 Broad Branch Road, N.W., Washington DC, 20015, USA

The present paper presents major element, trace element and Sr–Nd isotopic data from another peculiar assemblage of garnet pyroxenites. These rocks occur as layers and lenses within garnet-bearing high-temperature peridotite massifs from lower Austria (southern Bohemian massif). Taken together, equilibration temperatures higher than 1100–1400°C, pressures of ~3–3·5 GPa (~100–120 km), and geological and geochronological evidence indicate that the peridotite massifs represent fragments derived from the lithospheric mantle beneath a Devonian–Carboniferous convergent plate margin (Carswell, 1991; Becker, submitted). The lithological variability and trace element and isotopic compositions of the garnet pyroxenites provide independent evidence for a convergent margin setting. The data indicate that presumably CO_2-rich magmas strongly enriched in incompatible elements with radiogenic isotope signatures typical of Phanerozoic upper-crustal rocks must have once passed through the host peridotites at lower-lithospheric depths. These magmas were probably derived by melting of subducted continental crust in the sub-lithospheric mantle or received their crustal signature from fluids emanating from a subducted slab at greater depth.

GEOLOGIC SETTING

Garnet-bearing high-temperature peridotite massifs occur together with high-pressure granulite nappes in the high-grade Moldanubian zone of the southern Bohemian Massif (Fig. 1). In the Bohemian massif, early Carboniferous continental collision between the Baltic plate and rifted fragments of Gondwana resulted in top-to-the-NNE emplacement of the Moldanubian nappes onto the Moravo-Silesian foreland (Matte *et al.*, 1990). Shallow exhumation of granulites, peridotites and other Moldanubian units was interpreted to be a consequence of upper Visean (340–325 Ma) extensional collapse of the orogenic wedge (Matte *et al.*, 1990; Dallmeyer *et al.*, 1992). The peridotites are garnet lherzolites and spinel- and

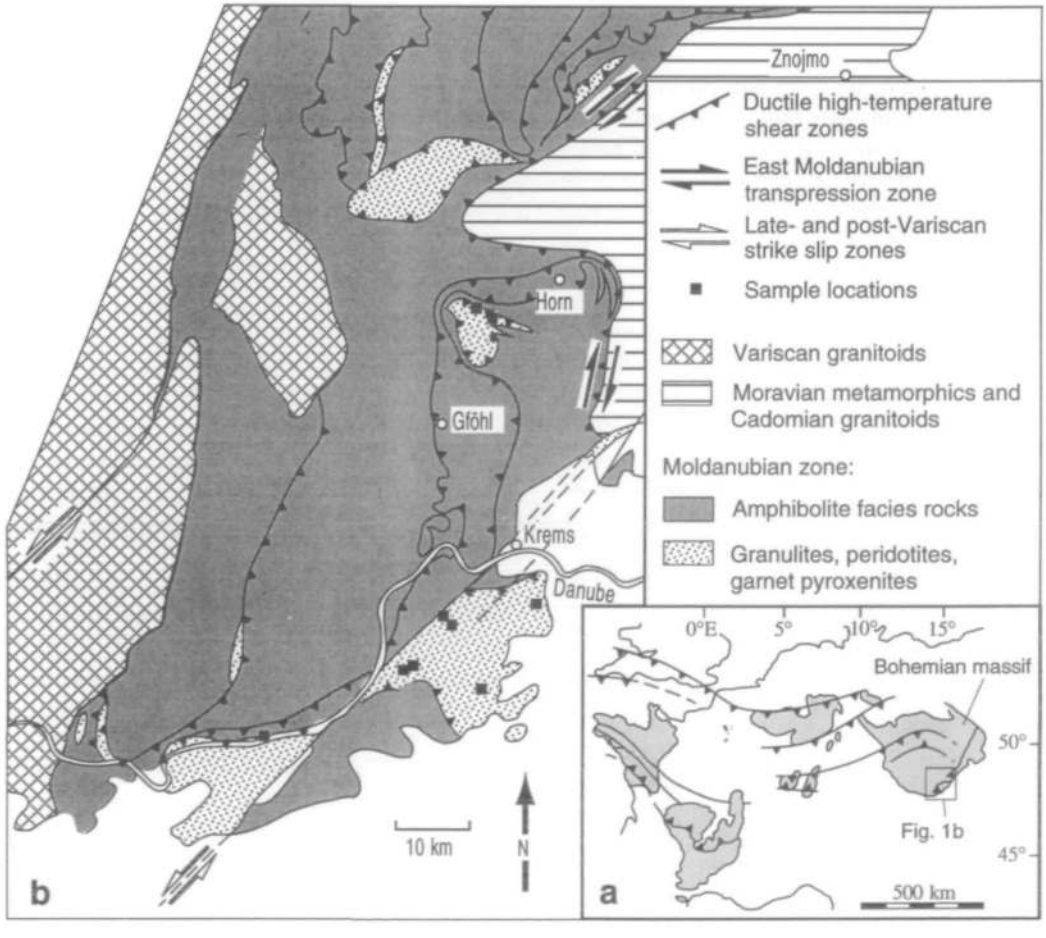

Fig. 1. (a) Tectonic map of the Variscan belt of central Europe. (b) Geological map of the lower Austrian and Czech part of the south-eastern Bohemian massif.

garnet-bearing harzburgites (Becker, 1996), and yield high equilibration pressures of ~3 GPa and temperatures of 1000–1100°C, estimated from mineral core compositions (Carswell, 1991). Equilibration temperatures of the garnet pyroxenites, also estimated from mineral core compositions, are similar or higher (1100–1200°C, Scharbert & Carswell, 1983; Becker, submitted). The bulk compositions of exsolved pyroxene megacrysts in some pyroxenites yielded primary crystallization temperatures of ~1400°C (Becker, submitted). Initial slow cooling at $T > 1200$°C is indicated by broad pyroxene exsolution lamellae in the pyroxene megacrysts, whereas Fe–Mg zoning in the garnets suggests high cooling rates (>150°C/Ma) during exhumation of the massifs ($T < 1200$°C). Geological and geochronological evidence suggests that the peridotite massifs represent fragments of mantle beneath a pre-Carboniferous marginal basin (Carswell, 1991; Becker, submitted).

SAMPLE SELECTION

The pyroxenites make up a few percent by volume of the ultramafic massifs. As a result of poor exposure and strong serpentinization of the peridotites, it is often difficult to assess the structural relation of the pyroxenites with their host peridotites. Hence, many of the samples used for this study are float blocks. However, some pyroxenites are concordant with the foliation of the host peridotite. Samples collected for this study include fresh garnet clinopyroxenites, some of them kyanite bearing, and garnet websterites, garnetites and some rocks that are physical mixtures of peridotites and pyroxenites. Pyroxene megacrysts occur either as constituents of pyroxenite layers or as lenses in harzburgite. The major element, trace element and isotopic compositions of the peridotites have been presented and discussed elsewhere (Becker, 1996). The samples were collected from the Kamptal peridotite massif (SL58, SL270), from peridotite massifs at Mitterbachgraben (DW231A, DW236), from outcrops near Schenkenbrunn (DW98, DW302B) and the Meidling (DW312, DW317, DW318, DW321, DW339, DW342) and Karlstetten quarries (WV1, WV2), and near Weitenegg (PW221). Outcrop locations are shown in Fig. 1, and latitude and longitude of outcrops have been given by Becker (1996). Details of the analytical techniques are given in the Appendix.

MAJOR AND TRACE ELEMENT VARIATIONS

Pyroxenite layers in ultramafic massifs rarely represent frozen melts as the pyroxenites often show considerable modal variability. A simple melting relationship is also not consistent with the zoned structure of some pyroxenite layers which have orthopyroxene-rich margins near the host peridotite and increasing modal abundance of clinopyroxene and garnet toward the centre of the layers (Kornprobst, 1969; Conquere, 1977*a*). The variability of compatible and moderately incompatible elements in pyroxenites coupled with their strong depletion in highly incompatible elements, particularly the large ion lithophile elements (LILE), cannot be produced by simple batch or fractional melting of a fertile or depleted peridotite (Suen & Frey, 1987). Experimentally produced partial melts of peridotite and natural melt compositions regarded as primitive are also compositionally different from mantle pyroxenites (Suen & Frey, 1987). On the basis of these observations, most workers agree that most pyroxenite layers found in peridotite massifs and xenoliths are formed by a combination of wallrock reaction and fractional crystallization of melts in the upper mantle (Green & Ringwood, 1967; Kornprobst, 1969; Conquere, 1977*b*; Suen & Frey, 1987).

Major elements

Selected major element variation diagrams for lower Austrian pyroxenites are illustrated in Fig. 2 (data in Table 1). The composition of the peridotites from lower Austria is shown for comparison. The samples in parentheses (also in Fig. 3) are rocks that are obvious mixtures of peridotite and millimetre-thick pyroxenite layers. Highlighted in Figs 2 and 3 (shaded field) are pyroxenites that show a relatively narrow range of isotopic compositions and are probably genetically related. These pyroxenites consist of garnet websterites, clinopyroxenites, garnetites and orthopyroxenites, and most of them have high MgO (>15 wt %). In samples with the highest MgO, the near-constancy in silica with decreasing MgO (Fig. 2a) is a consequence of the absence of cumulus garnet in the mineral assemblage close to the wallrocks (discounting the limited amount of garnet present owing to subsolidus exsolution). At lower MgO, SiO_2 drastically decreases owing to the appearance of garnet as a cumulus phase. This fractionation sequence is also present in modally zoned garnet pyroxenites, which show an increase of modal garnet from the wallrock to the centre of the pyroxenite dyke. The modal zoning of such pyroxenite dykes probably reflects reaction of high-temperature melts with the peridotite wallrock and subsequent partial freezing owing to conductive heat dissipation. In a diagram of CaO vs MgO (Fig. 2b), the pyrox-

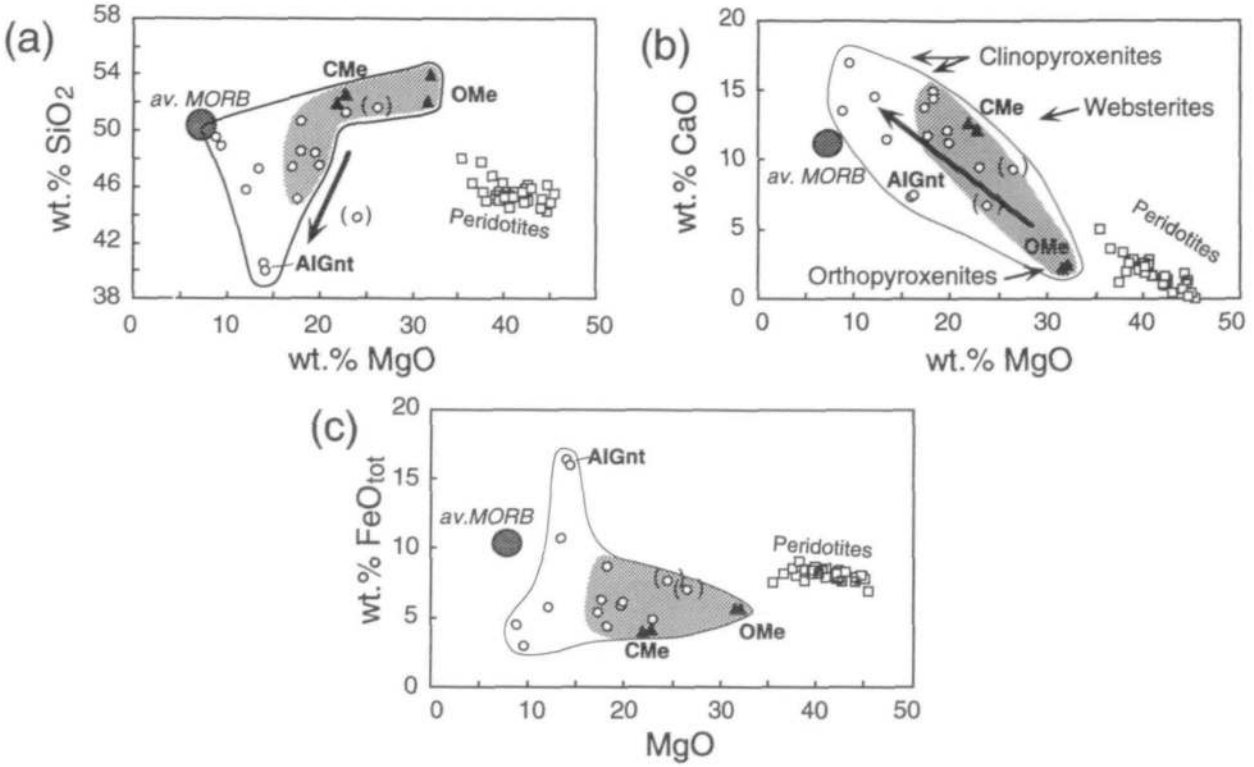

Fig. 2. Variation of selected major elements vs MgO in the pyroxenites (open circles). Cogenetic pyroxenites are highlighted by the shaded field. Samples in parentheses denote fine-grained interlayered peridotites and pyroxenites. CMe and OMe indicate clinopyroxene and orthopyroxene megacryst compositions (triangles). AlGnt indicates apatite–ilmenite garnetites. Arrows show wallrock reaction and fractionation trends as indicated from modally zoned pyroxenite layers. Average N-MORB composition (Hofmann, 1988) and variations shown by peridotites from lower Austria (Becker, 1996) are shown for comparison. (a) SiO_2 vs MgO. Strong decrease of SiO_2 at lower MgO indicates increasing amounts of garnet in the fractionation assemblage. (b) CaO vs MgO. Increasing CaO with decreasing MgO indicates clinopyroxene fractionation at decreasing temperatures. (c) FeO_{tot} vs MgO. All Fe calculated as FeO.

enites show an increase in CaO with decreasing MgO. This trend reflects both wallrock reaction (orthopyroxenites and websterites) and fractionation, the latter indicated by the variability of the clinopyroxenites. In contrast to the pyroxenites at high MgO, pyroxenites with lower MgO show larger variations in FeO content (Fig. 2c).

Minor and trace elements

Variations of some incompatible elements with MgO are shown in Fig. 3 (data in Table 2). Two distinct groups can be recognized in the plot of Na_2O vs MgO (Fig. 3a). Samples at high MgO have low Na_2O (<1 wt %), whereas the samples at low MgO generally have relatively high sodium (>1·5 wt %). As for FeO, the variation of Na_2O in MgO-rich samples is larger than in samples at low MgO. TiO_2 increases (Fig. 3b) in pyroxenites close to the wallrock (orthopyroxene to subcalcic clinopyroxene fractionation). Decreasing TiO_2 at lower MgO may reflect the temperature dependence of Ti substitution in garnet and pyroxenes during fractionation. The large variation of TiO_2 in pyroxenites at low MgO may be the result of variable proportions of minor Ti phases, but, as indicated by the similar behaviour of Na and Fe, perhaps also owing to compositional variations inherited from the parent melts. The rare earth elements (REE) Ce and Yb (Fig. 3c, d) show negative correlations with MgO at high MgO. The relatively large variation and the somewhat lower concentrations of the REE at low MgO reflect variable and more depleted melt compositions as compared with the pyroxenites at high MgO. It will be shown below that the low-MgO samples are not cogenetic, as they display large differences in isotopic composition.

RARE EARTH ELEMENTS

If the pyroxenites are cumulate rocks rather than crystallized melts, then their bulk-rock REE patterns are controlled by the REE patterns of the cumulus minerals. The REE abundances of the cumulus minerals, in turn, depend on the respective mineral–liquid partition coefficients and on the melt com-

Table 1: Major element analyses of garnet pyroxenites and megacrysts

Rock:	GPhlCp	GCp	Gnt	GCp	GWb	GCp	GCp	AlGnt	AlGnt	GCp
Eu anom.:	neg.	neg.	neg.	neg.	neg.	neg.	neg.	neg.	neg.	
Sample no.:	DW321A	DW321B	DW339B	DW339C2	DW339D	PW221	SL58	WV1	WV2	DW312
SiO_2	47·48	48·16	44·25	46·36	50·49	46·97	45·32	40·14	40·85	48·25
TiO_2	0·25	0·20	0·09	0·10	0·29	0·62	0·29	0·58	0·34	0·13
Al_2O_3	13·68	12·55	17·56	14·39	8·20	14·13	18·11	21·77	21·52	11·92
Cr_2O_3	0·38	0·36	0·15	0·17	1·10	0·05	0·08	0·02	0·03	0·29
Fe_2O_3							1·14			0·61
FeO	6·07	5·85	6·16	5·30	4·84	10·66	5·76	16·06	16·51	4·38
MnO	0·18	0·17	0·23	0·20	0·17	0·22	0·10	0·52	0·59	0·14
NiO	0·05	0·05	0·03	0·04	0·07	0·04	0·02	0·01	0·01	0·06
MgO	19·98	19·69	17·38	16·91	22·66	13·40	12·18	14·34	14·12	18·09
CaO	11·13	12·07	11·53	13·43	9·27	11·33	14·33	6·27	6·38	14·80
Na_2O	0·52	0·52	0·52	0·79	0·84	1·80	1·81	0·07	0·06	0·67
K_2O	0·18	0·01	0·01	0·01	0·02	0·07	0·02	0·01	0·01	0·02
P_2O_5	0·03	0·03	0·05	0·04	0·03	0·03	0·04	0·31	0·15	0·03
H_2O	1·02	0·60	1·30	0·84	0·90	0·29	0·22	0·36	0·34	0·45
CO_2	0·04	0·00	0·00	0·11	0·05	0·00	0·05	0·00	0·00	0·08
LOI	1·06	0·60	0·93	0·65	0·95					
Total	100·99	100·25	99·27	98·67	98·92	99·61	99·49	100·46	100·91	99·92
$Mg/(Mg+Fe^{2+})$	0·854	0·857	0·834	0·850	0·893	0·691	0·790	0·614	0·604	0·880
$Cr/(Cr+Al)$	0·026	0·028	0·008	0·011	0·112	0·004	0·005	0·001	0·001	0·024

Rock:	GCp	PxPe	OMe	OMe	CMe	CMe	GKyCp	GKyCp	PxPe
Eu anom.:			neg.	neg.	neg.		pos.		no
Sample no.:	SL270	DW302B	DW317A	DW317B	DW318	DW342	DW98	DW231A	DW 236
SiO_2	49·97	41·47	54·45	52·46	51·33	51·73	49·24	48·60	50·70
TiO_2	0·76	0·34	0·08	0·08	0·15	0·13	0·23	0·23	0·30
Al_2O_3	6·14	14·69	4·30	4·49	6·94	5·97	20·07	18·73	4·07
Cr_2O_3	0·20	0·22	0·83	0·83	0·85	0·98	0·04	0·06	0·36
Fe_2O_3							0·45	0·41	
FeO	8·54	7·27	5·65	5·66	3·95	4·02	4·49	2·96	6·89
MnO	0·18	0·36	0·13	0·13	0·12	0·12	0·09	0·07	0·16
NiO	0·08	0·08	0·11	0·11	0·08	0·07	0·02	0·02	0·14
MgO	18·00	23·27	32·62	32·02	21·65	22·53	8·84	9·47	26·08
CaO	14·15	6·65	2·42	2·21	12·46	11·93	13·36	16·73	9·11
Na_2O	0·70	0·49	0·10	0·10	0·80	0·71	2·59	1·97	0·43
K_2O	0·02	0·03	0·02	0·04	0·04	0·02	0·03	0·05	0·01
P_2O_5	0·02	0·02	0·02	0·02	0·02	0·02	0·02	0·01	0·01
H_2O	0·23	5·77	0·39	2·06	0·95	0·71	0·49	0·44	0·90
CO_2	0·19	0·12	0·09	0·09	0·05	0·09	0·00	0·08	0·00
LOI	0·42	5·89	0·27	2·06	0·60	0·42			0·90
Total	99·18	100·77	101·20	100·31	99·38	99·04	99·96	99·83	99·16
$Mg/(Mg+Fe^{2+})$	0·790	0·851	0·911	0·910	0·907	0·909	0·778	0·851	0·871
$Cr/(Cr+Al)$	0·031	0·015	0·150	0·145	0·104	0·132	0·002	0·003	0·079

G, garnet; Ky, kyanite; A, apatite; I, ilmenite; Phl, phlogopite; Cp, clinopyroxenite; Wb, websterite; Me, megacryst; Gnt, garnetite; PxPe, pyroxenite that contains thin peridotite layers. Total Fe calculated as FeO, except where Fe_2O_3 and FeO are given. LOI, loss on ignition.

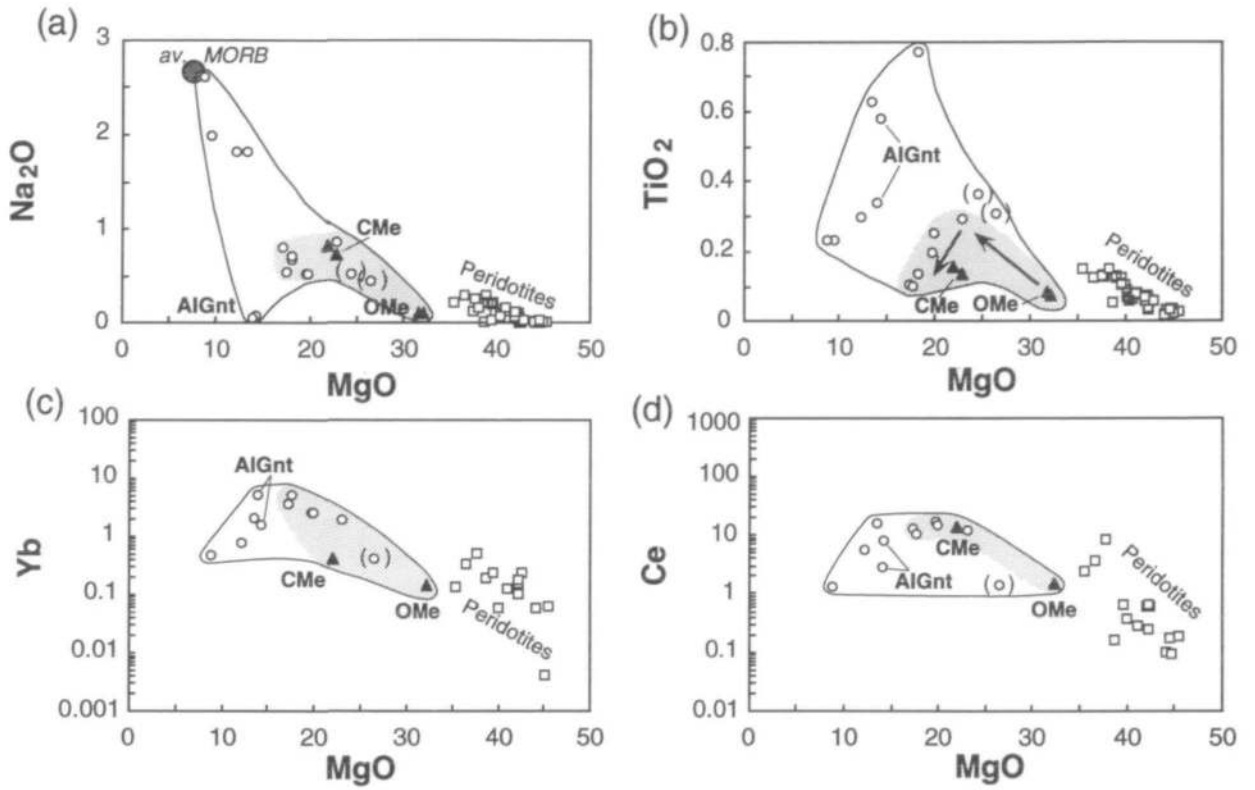

Fig. 3. Variation of some incompatible minor and trace elements in the pyroxenites. Abbrevations and symbols as in Fig. 2. (Note the large variations of Na_2O and TiO_2 at low MgO as compared with high-MgO samples. For more details, see text.)

position. Anhydrous pyroxenites from ultramafic massifs are generally depleted in LREE whereas amphibole- and mica-bearing pyroxenites often have flat or LREE-enriched patterns [see McDonough & Frey (1989) for a compilation]. In contrast, many anhydrous pyroxenites found as xenoliths in intraplate alkaline basalts and kimberlites show LREE-enriched or flat REE patterns which are interpreted as reflecting metasomatic processes in the lithosphere (McDonough & Frey, 1989). Figure 4 shows the REE patterns of garnet pyroxenites and two pyroxene megacrysts from lower Austria. From these patterns it is possible to distinguish four different pyroxenite groups, which are probably genetically unrelated to one another.

Figure 4a shows REE patterns of MgO-rich pyroxenites that are characterized by negative Eu anomalies and $(Tb/Yb)_n$ of unity, or less than unity depending on the amount of garnet present. The ratio of LREE/HREE scatters around unity but the $(La/Sm)_n$ ratio is always greater than unity. The latter reflects the strong LREE enrichment in the clinopyroxenes, which have Nd concentrations between 10 and 27 p.p.m. (Table 3). In all the whole rocks, La is somewhat depleted relative to Ce as a result of the high incompatibility of La in garnet (compare samples in Fig. 4a and b). Figure 4b shows bulk-rock REE patterns of exsolved pyroxene megacrysts. The LREE enrichment of the clinopyroxene megacryst is stronger than the LREE enrichment in the MgO-rich pyroxenites and the megacryst has $(Tb/Yb)_n > 1$. In the orthopyroxene megacryst, REE concentrations are lower and LREE enrichment is less pronounced than in the clinopyroxene megacryst. Clinopyroxene exsolved from the orthopyroxene megacryst also has high concentrations of Nd and Sm (Table 3) and an $(Sm/Nd)_n$ ratio ($\sim$0·8), similar to the bulk megacryst. Some of the pyroxenites with less MgO (sample PW221, Fig. 4c) have nearly flat REE patterns with only slight LREE enrichment and possess negative Eu anomalies. However, clinopyroxenes in this sample have high LREE abundances. The flat pattern of the bulk rock PW221 is simply a consequence of abundant modal garnet. The LREE enrichment and high abundances of LREE in these samples is unique compared with anhydrous pyroxenites from other peridotite massifs (McDonough & Frey, 1989).

Garnet clinopyroxenite sample SL58 has low MgO contents and a negative Eu anomaly, but

Table 2: Trace element analyses of garnet pyroxenites and megacrysts

Rock:		GPhlCp	GCp	Gnt	GCp	GWb	GCp	GCp	AlGnt	AlGnt
Eu anom.:		neg.	neg.	neg.	neg.	neg.	neg.	neg.	neg.	neg.
Sample:		DW321A	DW321B	DW339B	DW339C2	DW339D	PW221	SL58	WV1	WV2
Cr	XRF	2576	2493	1016	1136	7517	369	563	108	204
Ni	XRF	384	355	255	307	566	313	192	106	66
Co	XRF					39	59			63
	INAA	44·1	42·9	45	39·5	41·1	54·6	53	52·9	
Sc	INAA	71·2	68·1	107·8	71·9	43	43·6	38·8	47·8	
Zn	XRF	23	23			30	33	48	29	24
	INAA	30	30	19	28	28	31	65	25	
Cu	XRF					153	71		67	64
Cs	INAA	0·8		0·3				0·2	0·5	
Rb	XRF*	5					5			
	ID			0·254	0·256	0·637				
Ba	XRF	209	31			49	44		21	24
	INAA	168	41	37		73	60	23	36	
Sr	XRF	111	128			88	98	108	30	17
	ID			51·77	79·41	76·66				
Y		26	25			18	18	14	44	60
Zr	XRF	71	71			28	48	40	53	51
Hf	INAA	1·5	1·5			0·6	1·1	1·2	0·8	
Nb	XRF						3			
Ta	INAA	0·14	0·05	0·11	0·09	0·06	0·57	0·09	0·17	
V	XRF					216	316		332	249
Th	INAA	0·5	0·6	0·3	0·6	0·5	2·6	0·3	0·3	
U	INAA	0·3	0·3	0·5	0·3	0·2	1·6	0·8		
La	HPLC			3·34				1·51	3·487	0·967
	INAA	4·2	4·7	3	3·8	3·7	6·5	1·4	3·3	
Ce	HPLC			10·05				5·57	8·014	2·860
	INAA	14·8	16·7	11·6	12·3	11·3	15·5	4·9	7·3	
Pr	HPLC			1·42				1·08	1·043	0·510
Nd	HPLC			6·59				6·13	5·430	3·408
	INAA	11·5	16·9	4·1	5·5	6·7	8·3	8·1	5·2	
	ID			6·45	7·099	6·514		6·275		
SM	HPLC			1·46				2·01	2·544	2·478
	INAA	3·78	4·1	1·55	1·22	1·22	2·21	2·79	2·87	
	ID			1·5	1·235	1·211		2·59		
Eu	HPLC			0·335				0·526	1·181	1·055
	INAA	0·84	0·85	0·31	0·25	0·26	0·54	0·7	1·27	
Gd	HPLC			1·67				2·66	7·001	6·294
	INAA						2·8	3·9	7	
Tb	HPLC			0·424				0·459	1·626	1·510
	INAA	0·7	0·7	0·5	0·4	0·2	0·42	0·5	1·75	
Ho	HPLC			1·015				0·422	1·661	2·449
	INAA	0·8	1	1·1	1		0·8	0·6	1·8	
Er	HPLC			3·79				1·091	3·590	6·779
Tm	HPLC			0·607				0·141	0·467	0·947
	INAA	0·4	0·5	0·4	0·4	0·2	0·4	0·2	0·4	
Yb	HPLC			4·73				0·764	1·614	5·116
	INAA	2·5	2·4	4·3	3·4	1·9	2	0·7	1·4	
Lu	HPLC			0·747					0·204	0·755
	INAA	0·43	0·41	0·75	0·58	0·35	0·31	0·1	0·16	

Table 2: continued

Rock:		GCp	GCp	PxPe	OMe	CMe	CMe	GKyCp	GKyCp	PxPe
Eu anom.:					neg.	neg.		pos.		no
Sample:		DW312	SL270	DW302B	DW317A	DW318	DW342	DW98	DW231A	DW236
Cr	XRF	1997	1501	1505	5669	5813	6736	293	378	2494
Ni	XRF	483	648	591	894	599	552	191	135	1108
Co	XRF		62			34	36			74
	INAA					38·9		38·3		
Sc	INAA					30·9		26		
Zn	XRF	25	47	48	44	24	25	31	20	47
	INAA					29		41		
Cu	XRF		95				7			188
Cs	INAA					0·5		0·3		
Rb	XRF									
	ID				0·088			0·444		
Ba	XRF		161	49		67	25	37	33	
	INAA					44		20		
Sr	XRF	31	50	21	9	75	91	93	194	20
	ID				3·04					
Y		14	13	13		6	4	7	6	5
Zr	XRF	14	22	25	11	20	19	14	11	15
Hf	INAA					0·2		0·26		
Nb	XRF									
Ta	INAA					0·08		0·03		
V	XRF		393			148	149			271
Th	INAA					1		0·12		
U	INAA					0·9				
La	HPLC				0·666					0·512
	INAA					4·3		0·3		
Ce	HPLC				1·42					1·41
	INAA					13·3		1·3		
Pr	HPLC				0·184					0·241
Nd	HPLC				0·805					1·43
	INAA					6·4				
	ID				0·567			1·751		
Sm	HPLC				0·210					0·459
	INAA					1		0·92		
	ID				0·151			0·855		
Eu	HPLC				0·048					0·165
	INAA					0·22		0·46		
Gd	HPLC				0·185					0·628
	INAA					1·1				
Tb	HPLC				0·027					0·119
	INAA					0·2		0·19		
Ho	HPLC				0·041					0·159
	INAA					0·3		0·17		
Er	HPLC				0·121					0·519
Tm	HPLC				0·022					
	INAA							0·15		
Yb	HPLC				0·143					0·409
	INAA					0·4		0·47		
Lu	HPLC									0·064
	INAA					0·08		0·06		

Concentrations in p.p.m.* In most cases below detection limit (2 p.p.m.). XRF, X-ray fluorescence; INAA, instrumental neutron activation analysis; ID, isotope dilution; HPLC, high performance liquid chromatography.

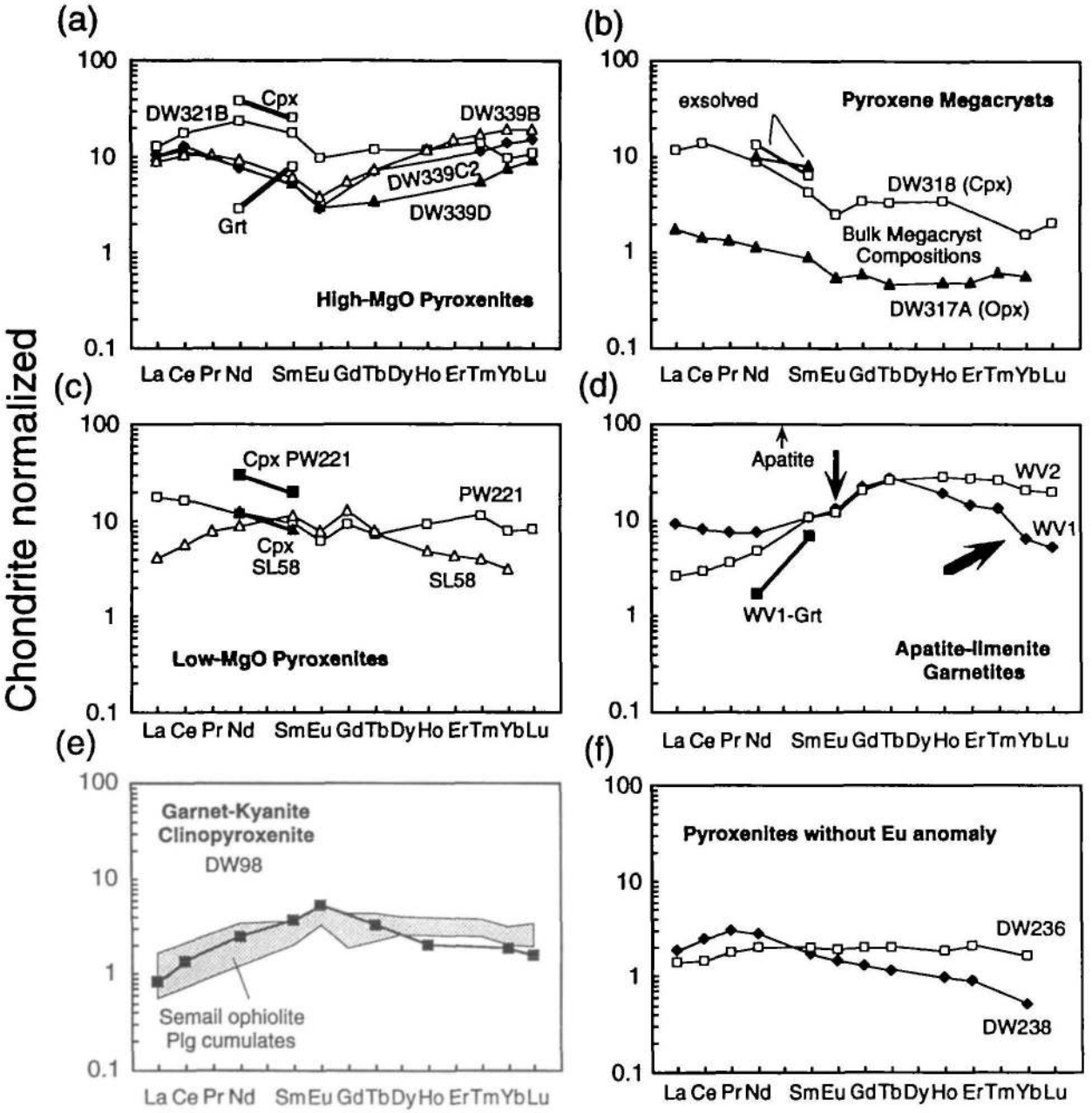

Fig. 4. Chondrite-normalized REE patterns of pyroxenites and megacrysts from lower Austria. The chondritic values of this and other REE diagrams are the CI values from Evensen *et al.* (1978) multiplied by a factor of 1·5. Arrows point to peculiar features. Cpx and Grt in (a) indicate normalized Nd and Sm concentrations (isotope dilution; ID) of clinopyroxene and garnet from garnet clinopyroxenite DW321B. Exsolved Cpx in (b) are normalized Nd and Sm concentrations (ID) of clinopyroxene exsolved from orthopyroxene megacryst sample DW317A and clinopyroxene megacryst DW318. Cpx in (c) are compositions of clinopyroxenes from samples PW221 and SL58. Apatite [not shown, arrow in (d)] has much higher Nd and Sm concentrations than garnet (Table 3). Shaded field in (e) gives a range of compositions of plagioclase-rich cumulates from the gabbroic section of the Semail ophiolite (Pallister & Knight, 1981). REE data of sample DW238 from Becker (1996).

displays convex upward REE patterns owing to a strong depletion in LREE and HREE (Fig. 4c). Apatite- and ilmenite-bearing garnetites show similar compositional features (Fig. 4d). Although one of these garnetites shows an LREE-depleted and HREE-enriched pattern as expected (WV2), the pattern of the other garnetite (WV1) is more complex. A strong fractionation of the MREE with

Table 3: Sr and Nd isotope and concentration data of garnet pyroxenites and megacrysts

Sample	Rock		$^{143}Nd/^{144}Nd$	$2\sigma_m$	ε_{Nd}	Sm (p.p.m.)	Nd (p.p.m.)	$^{147}Sm/^{144}Nd$	$^{143}Nd/^{144}Nd$ (335 Ma)	ε_{Nd} (335 Ma)	$^{87}Sr/^{86}Sr$	$2\sigma_m$	Sr (p.p.m.)	Rb (p.p.m.)	$^{87}Rb/^{86}Sr$	$^{87}Sr/^{86}Sr$ (335 Ma)
DW321A	GCp	Phl	0·511886	216	−14·7	0·022	0·074	0·1777	0·511496	−13·9	0·767305	12	16·54	74·3	13·000	0·705317
DW321B	GCp	Cpx,nm	0·512253	8	−7·5	5·939	27·32	0·1314	0·511965	−4·7	0·708763	11	251·6	0·0075	0·0001	0·708763
		Cpx,nm	0·512248	13	−7·6	4·894	22·62	0·1308	0·511961	−4·8	0·708748	14	215·5			0·708748
		Grt	0·513447	9	15·8	2·083	1·855	0·6792	0·511957	−4·9	0·708758	38	0·204	0·0039	0·0558	0·708492
		Grt*	0·513199	10	10·9	1·625	1·779	0·5521	0·511988	−4·3	0·708764	15	4·663	0·0217	0·0135	0·708700
		Amph	0·512293	13	−6·7	5·480	22·80	0·1453	0·511974	−4·5	0·708670	25	256·1	0·628	0·0071	0·708636
DW339B	Gnt	Cpx	0·512132	18	−9·9	1·665	12·89	0·0781	0·511961	−4·8	0·708768	13	156·4	0·0142	0·0003	0·708767
		WR				1·500	6·450	0·1406			0·708833	12	51·77	0·254	0·0142	0·708765
DW339C2	GCp	Cpx	0·512167	12	−9·2	1·160	9·553	0·0734	0·512006	−3·9	0·708716	15	131·9			0·708716
		WR				1·235	7·099	0·1052			0·708726	11	79·41	0·256	0·0093	0·708681
DW339D	GWb	Cpx	0·512234	12	−7·9	1·829	11·12	0·0994	0·512016	−3·7	0·708878	20	129·9	0·0032	0·0001	0·708878
		WR	0·512242	12	−7·7	1·211	6·514	0·1124	0·511995	−4·1	0·708903	23	76·56	0·637	0·0241	0·708788
DW339E	OMe	Cpx	0·512215	28	−8·3	2·070	10·85	0·1154	0·511962	−4·8	0·708827	15	113·2			0·708827
PW221A	GCp	Cpx (g)	0·512259	17	−7·4	4·681	20·90	0·1354	0·511962	−4·8	0·707659	11	171·3	0·0103	0·0002	0·707658
PW221B	GCp	Cpx (gr)	0·512275	10	−7·1	4·049	18·69	0·1313	0·511987	−4·3	0·707503	15	166·4			0·707503
SL58	GCp	Cpx	0·512381	12	−5·0	1·906	8·731	0·1320	0·512091	−2·2	0·705945	17	175·7	0·0366	0·0006	0·705942
		Cpx	0·512352	15	−5·6	1·780	8·134	0·1323	0·512062	−2·8	0·705883	13	159·6			0·705883
		Grt (c)*	0·513264	10	12·2	2·976	3·255	0·5528	0·512052	−3·0	0·705979	15	5·815	0·0112	0·0056	0·705952
		WR	0·512644	12	0·1	2·590	6·275	0·2495	0·512097	−2·1	0·70626	18	1080	20	0·0536	0·706004
WV1	AlGnt	Grt	0·513901	17	24·6	1·636	1·239	0·7986	0·512149	−1·1	0·706216	56	0·137	0·0048	0·1012	0·705734
		A	0·512380	11	−5·0	55·1	365	0·0913	0·512180	−0·5	0·705240	9	2390	0·0644	0·0001	0·705240
DW317A	OMe	Cpx	0·512371	13	−5·2	1·830	6·820	0·1622	0·512015	−3·7	0·708749	15	51·76	0·0030	0·0002	0·708748
		WR L	0·512425	12	−4·2	0·161	0·567	0·1715	0·512049	−3·1	0·709253	18	3·04	0·121	0·1148	0·708705
DW324A	CMe	Cpx	0·512215	17	−8·3	1·217	9·734	0·0756	0·512049	−3·1	0·708576	27	104·1	0·191	0·0053	0·708551
DW318	CMe	Cpx	0·512298	34	−6·6	1·473	9·391	0·0948	0·512090	−2·3	0·708208	15	123·1	0·0171	0·0004	0·708206
		Cpx	0·512267	20	−7·2	1·267	8·156	0·0939	0·512061	−2·8	0·707943	15				0·707943
		Amph	0·512237	107	−7·8	1·300	7·979	0·0985	0·512021	−3·6	0·713443	14	97·25	4·902	0·1469	0·712747
DW98	GKCp	Grt (c)*	0·512788	10	2·9	0·569	1·680	0·2048	0·512337	2·5	0·703695	13	6·392	0·0318	0·0144	0·703626
		WR	0·512904	16	5·2	0·855	1·751	0·2952	0·512257	1·0	0·704855	21	930	0·457	0·0142	0·704787
DW231A	GKCp	Cpx	0·513096	37	8·9	0·567	1·269	0·2701	0·512503	5·8	0·702798	44	59·23	0·1972	0·0096	0·702752
DW236	PxPe	Cpx	0·512895	21	5·0	1·227	3·612	0·2054	0·512444	4·6	0·703403	16	47·77	0·0017	0·0001	0·703403

Amph, amphibole; WR, whole rock; (c), core; (g), grey; (gr), green; *contains tiny inclusions; nm, non-magnetic fraction; L, leached whole rock; XRF data.

an abundance maximum near Tb is followed by a marked decrease from Tb to Lu. In addition, sample WV1 shows weak LREE enrichment from Nd to La; the HREE depletion evident in sample WV1 was verified by duplication with high performance liquid chromatography (HPLC) and instrumental neutron activation analysis (INAA) techniques (see Fig. A1, in the Appendix). The depletion of the HREE in samples SL58 and WV1 is surprising, as these samples are rich in cumulus garnet (~50 and 95 vol. %, respectively). This suggests that the magmas parental to these rocks already may have been depleted in HREE. The depletion in LREE just reflects the abundance of garnet. The low Sm/Nd ratios of clinopyroxenes (sample SL58) and apatites (sample WV1) from these rocks indicate that these minerals have LREE-enriched REE patterns (Table 3).

A garnet–kyanite clinopyroxenite from lower Austria has a positive Eu anomaly and exhibits LREE and HREE depletion (Fig. 4e). The REE pattern of sample DW98 shows similarities to the patterns found in some Al- and Ca-rich garnet pyroxenites from Ronda and Beni Bousera in that these samples also have positive Eu anomalies and low REE abundances (Suen & Frey, 1987; Kornprobst *et al.*, 1990). Figure 4e shows a comparison with REE data (shaded field, Pallister & Knight, 1981) from cumulate gabbros from the Semail ophiolite (Oman). There is a marked similarity between the garnet–kyanite clinopyroxenites from lower Austria (see also sample DW231A, Tables 1–3) and these plagioclase cumulates not only with respect to REE but also with respect to the major and other trace elements (Smewing, 1981). However, the garnet–kyanite clinopyroxenites do not contain primary plagioclase.

Some pyroxenites from lower Austria are characterized by the absence of Eu anomalies, low REE abundances (0·5–3 times chondrites) and variable REE patterns (flat to LREE enriched; Fig. 4f). These garnet clinopyroxenites and websterites are rich in MgO and form millimetre- to centimetre-thick bands interlayered with LREE-depleted peridotites at the Mitterbachgraben locality.

NORMALIZED ELEMENT CONCENTRATION DIAGRAMS

The element abundances are illustrated in Fig. 5 normalized to primitive mantle abundances. The elements are arranged in order of increasing bulk partition coefficient during melting in the suboceanic mantle (Hofmann, 1988). Figure 5a shows trace element patterns for MgO-rich pyroxenites with negative Eu anomalies. These rocks have marked negative K, Rb, Ta, Ti and P anomalies. Weak negative Sr anomalies are present but are not so obvious owing to the strong adjacent P anomaly. Potassium and Rb are always strongly depleted but Ba may be enriched to a certain degree. The trace element pattern of a clinopyroxene megacryst (Fig. 5b) is similar to that of the MgO-rich pyroxenites in Fig. 5a. One of the MgO-rich pyroxenites (DW321) has been locally altered by retrograde interaction with a high-temperature metasomatic fluid, presumably derived from the surrounding felsic granulites (Becker & Wenzel, 1996). This alteration led to the formation of phlogopite and resulted in higher K, Ba and Rb abundances of the altered portions of the rock (compare samples DW321A and B in Tables 1 and 2).

Pyroxenites with low MgO (samples PW221 and SL58, Fig. 5c) also have negative Ti, P, Zr and Hf anomalies (relative to Sm and Gd or Tb), but these anomalies are much less pronounced than those exhibited by the MgO-rich pyroxenites. The somewhat higher Rb and K abundances in sample PW221 reflect the presence of minute quantities of retrograde phlogopite that formed from an extraneous metasomatic fluid, similar to phlogopite in sample DW321A (Tables 1 and 2). In common with the MgO-rich pyroxenites, samples PW221 and SL58 are depleted in K. In contrast to the MgO-rich pyroxenites, Ta shows only a weak depletion relative to the MREE in sample SL58 and is enriched in sample PW221. Sample SL58 contains a few tiny rutile grains that are only found enclosed in garnet, whereas sample PW221 contains interstitial ilmenite grains in the matrix. Th concentrations in sample PW221 are very high, probably owing to tiny inclusions of Th-rich accessory minerals in garnet (indicated by yellow halos).

Normalized element concentration diagrams for bulk rocks from two apatite–ilmenite garnetites are shown in Fig. 5d. Negative Ti and Zr anomalies are present, but are much less pronounced than in the MgO-rich pyroxenites, presumably owing to the presence of ilmenite in the garnetites. Phosphorus shows a positive anomaly in the garnetites owing to the presence of apatite inclusions. Tantalum is not depleted relative to the LREE because the latter also are depleted. Despite the presence of apatite inclusions, the garnetites display negative Sr anomalies.

The garnet–kyanite clinopyroxenite shown in Fig. 5e is distinct from the other clinopyroxenites in that it has positive Sr, Eu and Ba anomalies. It is important to recall in this context that sample DW98 has an unusual mineralogy which, besides Ca-rich garnet and clinopyroxene, includes primary

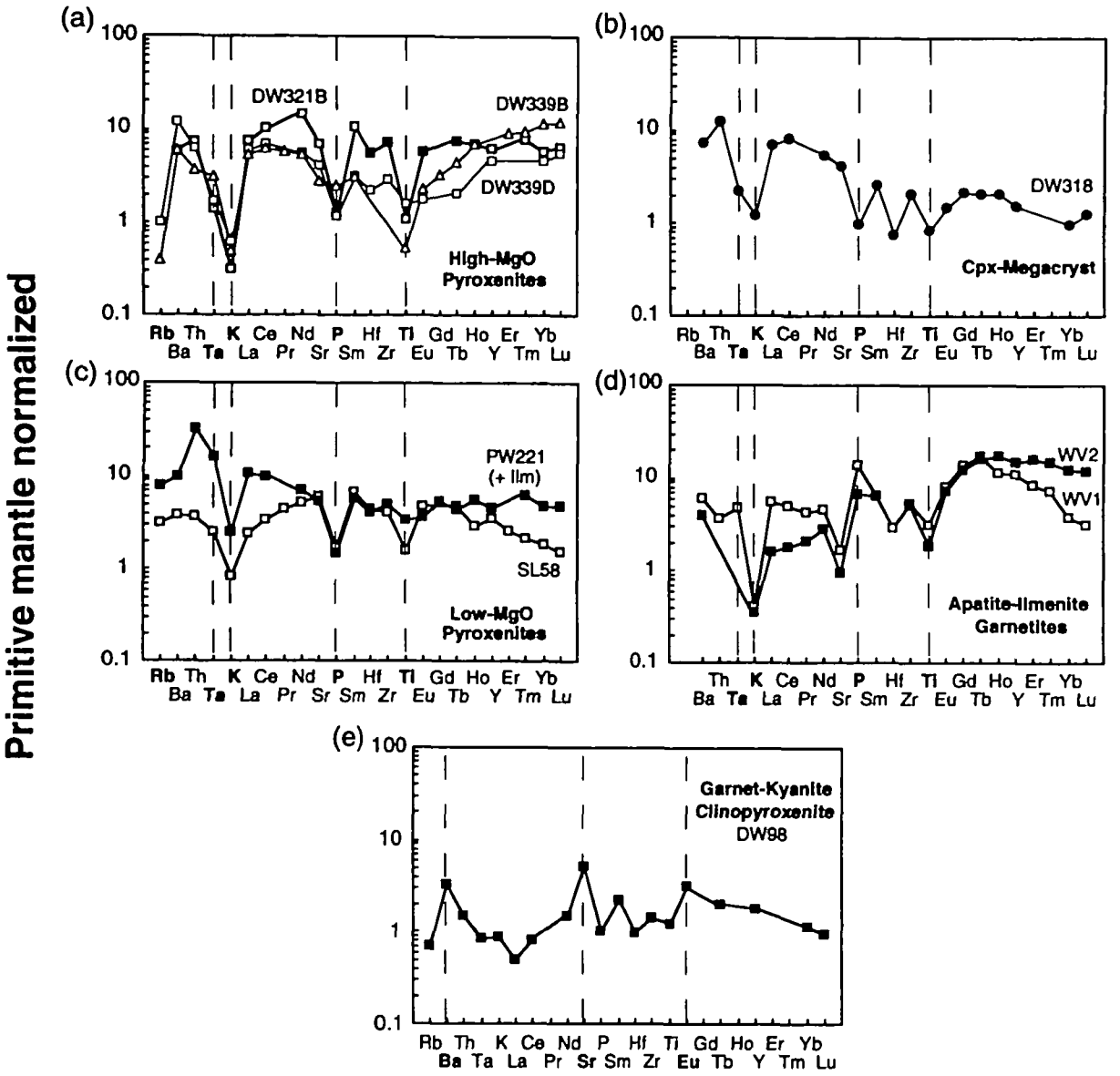

Fig. 5. Primitive mantle normalized element concentration diagrams of the pyroxenites. Normalizing values and compatibility sequence from Hofmann (1988), except Rb, K (McDonough *et al.*, 1992), and P (Sun & McDonough, 1989). In these diagrams Ti, P, K, Y, Zr, Sr and Ba are XRF data (Ba also INAA), Th, Ta and Hf are INAA data, REE are INAA, HPLC and ID (Nd, Sm) data, and Rb is ID data (except Rb of PW221 and SL58, which are XRF data). The extent of negative Ti–Ta–P anomalies is related to the presence or absence of Ti and P phases. (Note the strong depletion of K and Rb relative to La and the high Th abundances of most pyroxenites.)

kyanite and rutile. These kyanite-bearing samples (also sample DW231A) are also distinguished by high Ca contents, the highest Al and Na and lowest Mg, Ni, Cr, Sc and Zr contents of all the pyroxenites investigated (Tables 1 and 2).

Sr AND Nd ISOTOPIC COMPOSITIONS

Sr and Nd isotope data for clinopyroxenes, garnets, whole rocks and retrograde minerals from lower Austrian garnet pyroxenites and megacrysts are presented in Table 3. The data are plotted in the form of an ε_{Nd}–$^{87}Sr/^{86}Sr$ diagram in Fig. 6a, with data from the peridotites (Becker, 1996) shown for comparison. The Sr and Nd isotope ratios have been corrected for radioactive decay to 335 Ma based on cooling ages obtained on pyroxenites and peridotites (344–325 Ma; Becker, submitted). Some geochronological evidence indicates calcalkaline magmatism in

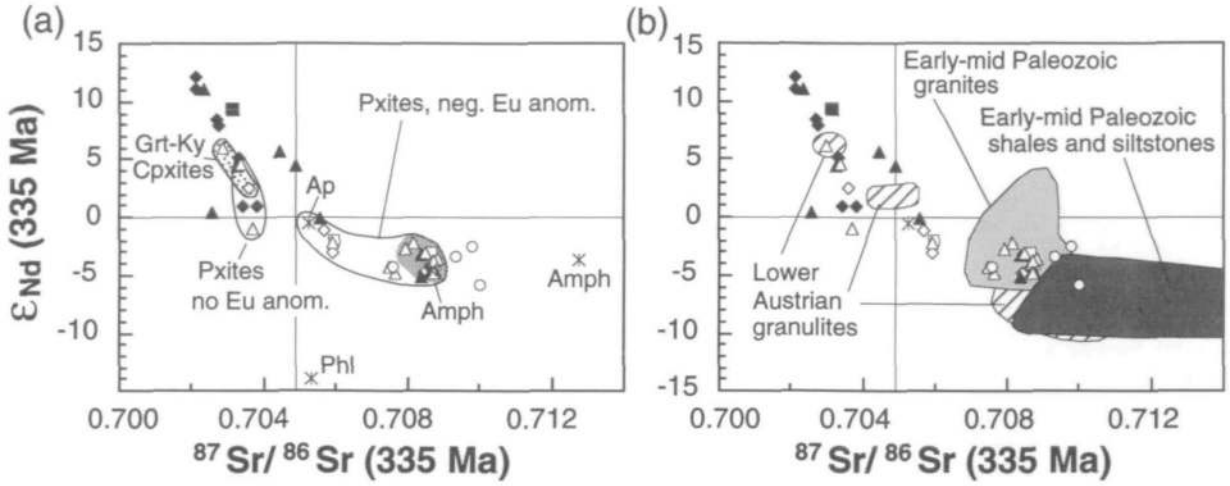

Fig. 6. ε_{Nd}–$^{87}Sr/^{86}Sr$ diagram calculated at 335 Ma. Shown are mineral and whole-rock isotope data of pyroxenites and megacrysts (open symbols) and data from peridotites (solid symbols; Becker, 1996) whole-rock data of calc-silicate marble and enclosed pyroxenites (open circles, H. Becker, unpublished data, 1996). Garnets are shown as diamonds, clinopyroxenes as triangles, whole rocks as squares and the crosses are apatite (Ap), secondary amphibole (Amph), or secondary phlogopite (Phl). Other abbreviations as in Fig. 2. In (a) three different types of pyroxenites, as indicated by the presence or absence of Eu anomalies (Fig. 3), are distinguished. Errors are similar (Nd) or smaller (Sr) than size of symbols. (b) Data from (a) in comparison with high-pressure granulites from lower Austria (H. Becker, unpublished data, 1996) and Palaeozoic sediments and granites (Davies *et al.*, 1985; Liew & Hofmann, 1988; Stosch & Lugmair, 1984).

southern Bohemia at 360–380 Ma, shortly before collision (Kosler *et al.*, 1993; Wendt *et al.*, 1994). It is possible that the pyroxenite layers are related to this igneous activity. That the pyroxenite layers have only spent a short period of time in the deep lithospheric mantle is also indicated by the observed small-scale isotopic disequilibrium across modally zoned pyroxenite layers (samples DW339, PW221). It might perhaps be more appropriate to make the age correction back to 360 Ma rather than 335 Ma, but the difference of 20–50 Ma has little effect on the initial Sr and Nd isotopic ratios. Even if the pyroxenites are much older, their initial $^{87}Sr/^{86}Sr$ would not change substantially owing to the very low Rb/Sr. Figure 6a also shows the isotopic composition of retrograde amphiboles and a retrograde phlogopite from two MgO-rich pyroxenite samples. One of the amphiboles is in isotopic equilibrium with anhydrous pyroxenite minerals at 335 Ma, whereas the other has a higher Sr isotopic composition compared with clinopyroxenes and garnets. The phlogopite from sample DW321A has a different Sr and Nd isotopic composition compared with clinopyroxenes from the unaltered portion of the rock (DW321B, Table 3). In fact, the phlogopite may be slightly younger than 335 Ma, and the low $^{87}Sr/^{86}Sr$ may be the result of a wrong age correction and the high Rb/Sr of the phlogopite.

Most of the minerals from lower Austrian peridotites (filled symbols in Fig. 6) have high ε_{Nd} and low $^{87}Sr/^{86}Sr$ and are thus similar to depleted mid-ocean ridge basalts (Becker, 1996). However, the observed variation particularly of the Nd isotopes is very large, and a few samples extend the spread to high $^{87}Sr/^{86}Sr$ ratios and low ε_{Nd}. These latter samples show petrographical evidence for physical mixing of peridotites with pyroxenite layers. Mineral separates from the MgO-rich pyroxenites with negative Eu anomalies and the pyroxene megacrysts have very radiogenic Sr isotope ratios (0·7075–0·7089) and negative ε_{Nd} (−2·3 to −4·8) values. Such isotopic compositions are similar to or even higher than those of certain arc basalts, for example, from the Sunda–Banda island arc (Edwards *et al.*, 1993) and the Lesser Antilles island arc (White & Dupre, 1986). Isotope signatures such as these have been interpreted to reflect the presence of minor amounts of a sedimentary component derived from the subducting slab. A pyroxenite with low MgO and a negative Eu anomaly (SL58) and the apatite–ilmenite garnetites (WV1 and 2) have significantly lower $^{87}Sr/^{86}Sr$ (0·7052–0·7059) and higher ε_{Nd} (−0·5 to −2·2) than the MgO-rich pyroxenites. Apparently, the parent melts of the pyroxenites with low MgO must have been derived from sources with higher proportions of material showing long-term depletion in incompatible elements.

Figure 6b shows a comparison of the pyroxenites and peridotites from lower Austria with the isotopic compositions of early- to mid-Palaeozoic sediments and granites. Also shown is the compositional range of mafic and felsic granulites from lower Austria (H. Becker, unpublished data, 1996). A contribution from upper-crustal rocks is indicated by the simi-

larity in isotopic compositions of the MgO-rich pyroxenites and high-temperature pyroxene megacrysts to Palaeozoic sediments and granites. Whole-rock isotopic compositions of high-pressure, high-temperature calc-silicate rocks found close to a peridotite outcrop in lower Austria (Becker & Altherr, 1992; H. Becker, unpublished data, 1996) are even more radiogenic in Sr and have somewhat lower ε_{Nd} than the MgO-rich pyroxenites (Fig. 6a). The isotopic and trace element compositions of the calc-silicate rocks suggest that they are not genetically related to the cumulus pyroxenites discussed here, although they seem to have equilibrated at the same depth.

Both the pyroxenites without Eu anomalies (Mitterbachgraben locality) and those with positive Eu anomalies have isotopic compositions very different from the pyroxenites with negative Eu anomalies (Fig. 6a). Apart from the trace element variations, the isotopic compositions also preclude any simple genetic relationships between these rocks. The pyroxenites without Eu anomalies and those with positive Eu anomaly have low, but mostly positive ε_{Nd} (the former 4·6 to −1·1, the latter 5·8 to 2·5) at relatively low $^{87}Sr/^{86}Sr$ (0·7028–0·7037). The pyroxenites without Eu anomalies and their peridotite host rocks (Mitterbachgraben locality) define an isotopic trend from compositions similar to mid-ocean ridge basalt (MORB) to low ε_{Nd} at low $^{87}Sr/^{86}Sr$.

CONSTRAINTS ON EQUILIBRIUM MELT COMPOSITIONS

Accessory mineral control on trace element abundances of the cumulates

Abundances of most incompatible trace elements in the pyroxenite bulk rocks have not been substantially affected by retrograde metamorphic processes. As the abundance of amphibole and even rarer phlogopite is <0·5–1 vol. %, and concentrations, for example, of Sr and Nd in amphibole are similar to those in clinopyroxene (Table 3), retrograde amphibole cannot account for the enrichment in incompatible elements observed in pyroxenite bulk rocks. Tiny inclusions (10–30 μm) with high refractive indices are found predominantly in cumulus garnets from some of the pyroxenites. Some of these inclusions have yellow halos, a feature that is known from monazite inclusions in garnet (K. Mezger, personal communication, 1995). If these inclusions are indeed monazite they may have a major influence on the Th and REE concentrations of the bulk rocks. Unfortunately, it is not possible to obtain a reliable estimate for the weight fraction of these minerals because of the very small quantities and their heterogeneous distribution. Some thin sections contain no more than a few grains of these mineral(s) and hence they are easily overlooked. Rudnick *et al.* (1993) reported relatively large monazite inclusions (~100 μm) in olivine from a metasomatized harzburgite xenolith. These monazites contain 9 wt % Th and demonstrate that minerals with extremely high Th and REE abundances can exist in the mantle.

To evaluate the possible influence of accessory minerals on abundances of highly incompatible elements, mass balance calculations were done for some pyroxenite and megacryst samples. The calculated Th concentrations of the bulk rocks (not shown) based on reasonable assumptions for concentrations in garnet and pyroxenes [see data of Tatsumoto *et al.* (1992)] are an order of magnitude lower than the observed bulk-rock concentrations measured by INAA. Deficiencies between calculated and measured bulk-rock Nd and Sm abundances may indicate that the small inclusions also contribute to the REE budget of the bulk rocks. Alternatively, it is also possible that the mineral separates were partially dissolved during the leaching procedure, leading to the observed deficiencies. Titanium minerals are present in some pyroxenites and in the apatite–ilmenite garnetites. Rutile occurs as rare solitary inclusions (up to 50 μm) in garnets and pyroxenes in websterites and clinopyroxene megacrysts. The prismatic and rounded shapes are not consistent with an origin by exsolution. In some clinopyroxenites (samples DW98, PW221, SL270) and in the apatite–ilmenite garnetites (WV1 and WV2), rutile or ilmenite are more abundant, occur along grain boundaries, and have grain sizes typically between 100 and 200 μm. These minerals are potentially important for the high field strength element (HFSE) budget as they have high partition coefficients for these elements (Green & Pearson, 1987). Apatite is present only as a minor phase in garnetite samples WV1 and WV2, where it serves as an important host for Sr, LREE (Table 3) and Th.

Melt compositions in equilibrium with pyroxenites and pyroxene megacrysts

By dividing the element concentrations in the pyroxenites by their bulk distribution coefficients, it is possible to calculate the compositions of melts in equilibrium with the pyroxenites. For this to be meaningful, the pyroxenites are required to be true cumulates that do not contain interstitial melt. The observation that in the MgO-rich pyroxenites the

normalized abundances of K and Rb are a magnitude lower than La abundances (Fig. 5) supports this suggestion. Terrestrial magmas with high LREE and Th abundances have similar or higher normalized abundances of K and Rb (except for some carbonate-rich magma types). Trapped interstitial melt would have resulted in K and Rb abundances in the pyroxenites higher than actually observed. Although the presence of igneous layering and the depletion in K and Rb are consistent with a cumulus origin, in the previous section it was shown that very small quantities of accessory minerals (monazite?) may control abundances of Th and perhaps also Ta (rutile). In contrast, the REE budget of all pyroxenites and megacrysts is dominated by the REE in pyroxenes and garnet, except for some garnetites where apatite is also important (Table 3). In these cases, only a maximum of 10–25% of the REE in the bulk rocks can be accounted for by monazite inclusions. Therefore, despite this caveat, the REE can be used to estimate the possible REE patterns of melts in equilibrium with the pyroxenites and megacrysts.

The weight fractions of the respective minerals in the pyroxenites were calculated from the normative abundances of garnets, pyroxenes and minor mineral phases. Mineral–liquid partition coefficients used in the calculations are compiled in Table 4. To reduce uncertainties with respect to relative element partitioning, garnet and pyroxene partition coefficients were taken from a few recent experimental studies that yielded a large number of $D^{(min/l)}$ values relevant for melting processes in the upper mantle (Beattie, 1993*a*, 1993*b*; Johnson, 1993; Hart & Dunn, 1993; Kelemen *et al.*, 1993, and references therein). These D values are at present the most reliable ones because the run products of partitioning experiments were analysed using ion microprobe techniques with low detection limits and high precision. Partition coefficients for accessory minerals are often much more poorly known, and are also given in Table 4. Figure 7a shows calculated equilibrium melt compositions of the MgO-rich pyroxenites and pyroxene megacrysts. The strong LREE enrichment and fractionation from the MREE should be noted [$(La/Sm)_n = 7–47$; Table 5]. Even if one takes into account that monazite may contribute up to 25% (which is probably too high) to the LREE budget of sample DW321B, this would reduce the abundance of La only from 600 times the chondritic value to 450 times the chondritic value. Clinopyroxenes from the garnet pyroxenites also show strong enrichment in LREE and Sr, indicating that clinopyroxenes act as the major control on bulk-rock LREE abundances (Table 3). For instance, clinopyroxenes from the garnet websterite sample

Table 4: Mineral–melt partition coefficients

	Garnet	Cpx	Opx	Rutile	Ilmenite	Apatite
Th	0·0015	0·0013	0·00003	0·01*	0·01*	1·3
Ta	0·007	0·0077	0·003	5	4	0·001*
La	0·001	0·0536	0·0005	0·1*	0·01*	2·8
Ce	0·005	0·0858	0·0009	0·1*	0·01*	3·5
Nd	0·04	0·1875	0·009	0·1*	0·01*	4·2
Sr	0·0008	0·1283	0·0005	0·01*	0·01*	1·1
P	0·15/0·01	0·0067	0·001	0	0	—
Sm	0·22	0·291	0·02	0·1*	0·01*	4·5
Zr	0·34	0·1234	0·014	5	0·27	0·05
Ti	0·45	0·384	0·14	—	—	0·05
Eu	0·6	0·35	0·03	0·1*	0·01*	1·1
Tb†	1·4	0·405	0·05	0·1*	0·01*	4·25
Y	3·1	0·467	0·18	0·2*	0·01*	2
Er	3·5	0·42	0·07	0·2*	0·01*	3
Yb	4	0·43	0·1	0·2*	0·01*	2·2
Sc	8·5	1·31	0·8	0·2*	0·2	0·05
Cr	4	3·8	1·9	10	6	0·05
Ni	5·1	2	3	0·5*	1	0·12

Sources of partition coefficients are as follows. *Garnet*—Shimizu & Kushiro (1975), Beattie (1993*b*), Johnson (1993). Value for Ta is poorly known; instead, Nb value of Johnson (1993) was used. P is 0·15 for basalts from Thompson (1975), 0·01 for carbonatites (Baker & Wyllie, 1992); Sc, Cr and Ni from Irving (1978), Irving & Frey (1978) and A. Fett (personal communication, 1994*a*). *Clinopyroxene*—Beattie (1993*a*), Hart & Dunn (1993); for Ta the Nb value of Hart & Dunn (1993) was used; P from Baker & Wyllie (1992); Ni from Irving (1978). *Orthopyroxene*—Irving (1978), Baker & Wyllie (1992), Beattie (1993*a*), Kelemen *et al.* (1993); Ta assumed based on Nb value of Kelemen *et al.* (1993). *Rutile–ilmenite*—Ta: rutile basalt, Wendlandt (1990), McCallum & Charette (1978), A. Fett (personal communication, 1994). *Apatite*—Benjamin *et al.* (1980), Watson & Green (1981), Irving & Frey (1984), O'Reilly *et al.* (1991), Porcelli *et al.* (1992), Hauri *et al.* (1993).
*Assumed value, based on crystal structure considerations.
†Values for Tb estimated from Gd and Dy data.

DW321B have Nd abundances ~40 times the chondritic value (Fig. 4a). Using the clinopyroxene–melt partitioning coefficient of Hart & Dunn (1993), equilibrium melts must have contained about five times more Nd than the clinopyroxenes, which is in good agreement with the calculation for the bulk rock (Fig. 7a). Orthopyroxene megacrysts do not yield evidence for an accessory phase control of their LREE budget, but show the same type of REE pattern for a calculated equilibrium melt also with high abundances of LREE and high $(La/Sm)_n$ and $(La/Yb)_n$. Calculated melt compositions for apatite–ilmenite garnetites (Fig. 7b) show strong LREE–HREE fractionation and more variable LREE abundances than the MgO-rich pyroxenites. Figures

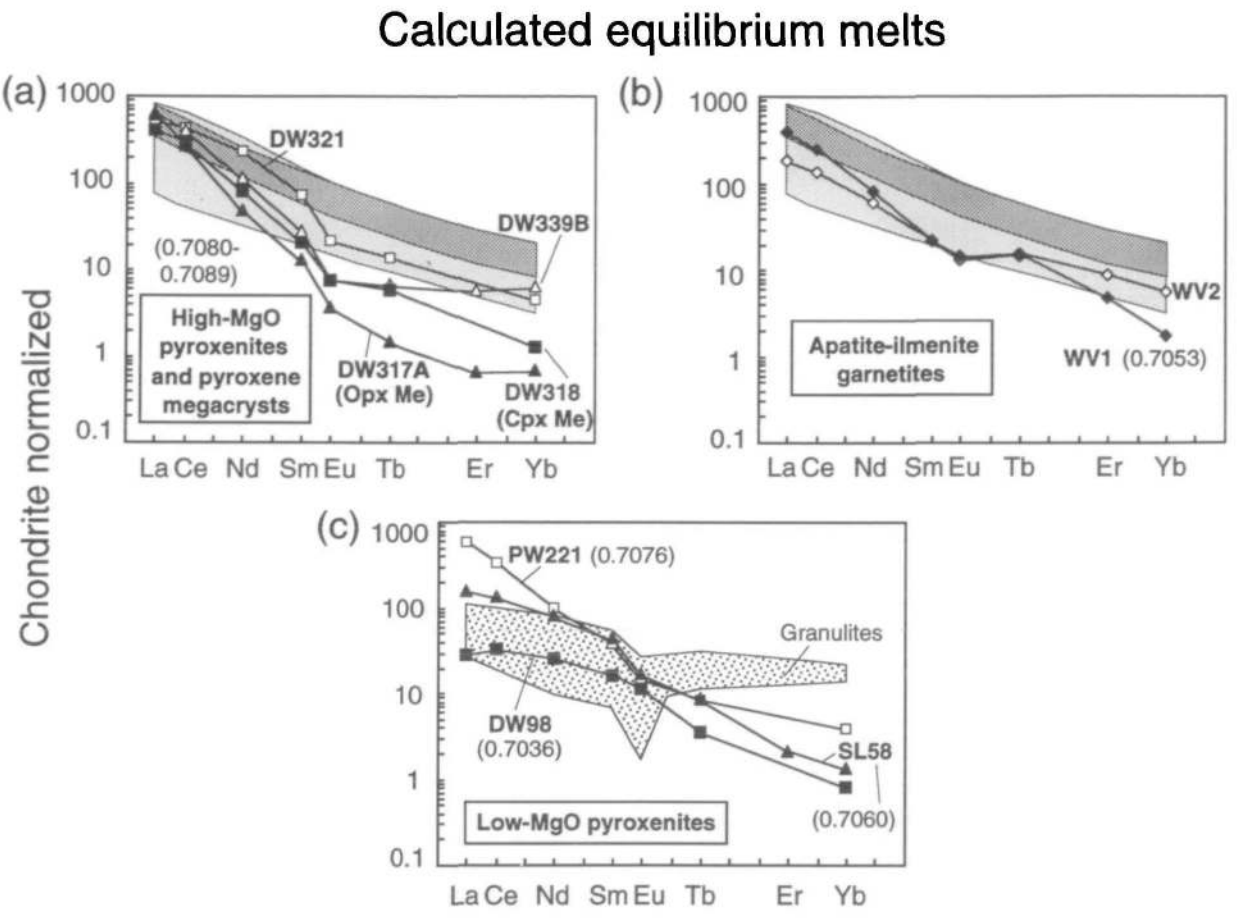

Fig. 7. Chondrite-normalized REE patterns of melts in equilibrium with pyroxenites and megacrysts. Patterns were calculated using cumulate compositions and mineral–liquid partition coefficents in Table 4. Also given are $^{87}Sr/^{86}Sr$ (335 Ma) ratios of pyroxenites and megacrysts. For comparison, range of REE patterns of European melilitites (dark grey; Alibert *et al.*, 1983) and ranges of kimberlites and alnöites (light grey; Hearn, 1989) are shown in (a) and (b). Range of REE patterns (stippled field) of mafic and felsic granulites from lower Austria is given in (c).

7a and b also show ranges of REE patterns of continental intraplate melilitites, kimberlites and alnöites. Compared with these melts, the LREE enrichment and LREE–MREE fractionation of equilibrium melts of the pyroxenites are similar or even greater.

Calculated melts in equilibrium with the pyroxenites with low MgO (Fig. 7c) show more variable LREE enrichments and fractionation. The REE pattern of the equilibrium melt of sample PW221 looks similar to that of melts in equilibrium with the MgO-rich pyroxenite suite. Similar isotopic compositions may indicate genetic relationships. Melts equilibrated with samples SL58 and DW98 have lower LREE/MREE ratios but are more strongly fractionated with respect to the HREE. It appears that the strong LREE–HREE fractionation is a primary characteristic of the equilibrium melts, as is also the case for the Eu anomalies. Figure 7c also shows a range of REE patterns of mafic to felsic high-pressure granulites (H. Becker, unpublished data, 1996). The granulites show much weaker LREE–MREE fractionations and lower La and Ce abundances than the calculated equilibrium melts of the pyroxenites. This appears to rule out a direct genetic relationship between the granulites and these melts.

TiO_2 and P_2O_5 saturation in equilibrium melts?

Calculation of equilibrium melt abundances for HFSE is fraught with much larger uncertainties than calculation of REE abundances because of the presence of minor and trace amounts of Ti and P minerals. The presence of Ti minerals suggests that equilibrium melts were saturated in Ti. However, the high solubility of Ti in basaltic magmas at high

temperatures (~9 wt% TiO_2 at 1400°C; Green & Pearson, 1986; Ryerson & Watson, 1987) and the relatively low TiO_2 contents of basaltic magmas erupted at the surface suggest it is unlikely that basaltic magmas ever reach Ti saturation (Green & Pearson, 1986; Ryerson & Watson, 1987). Silicic melts have very low Ti solubilities. However, it is difficult to imagine that such melts can travel very far in a mantle at 1100–1400°C without reacting with the mantle. Such melts would become magnesian as a result of reaction with peridotite and would have higher Ti solubilities. The same may be true for phosphorus. Apatite is present in significant amounts in the apatite–ilmenite garnetites, indicating P saturation in the corresponding melt. At temperatures of 1400°C up to 7 wt% P_2O_5 can be dissolved in a basaltic melt (Harrison & Watson, 1984), much more than measured in any basaltic lava.

Carbonatites have low solubilities of TiO_2 (~1–1·2 wt% at 1150–1180°C; Wallace & Green, 1988; Baker & Wyllie, 1992), as is also indicated by strong negative Ti anomalies of carbonatites (Nelson *et al.*, 1988). Furthermore, carbonatites can dissolve large amounts of P_2O_5 (Baker & Wyllie, 1992). The presence of large amounts of CO_2 in silicate melts can strongly reduce TiO_2 solubility. For example, ilmenite coexists with CO_2-rich alkaline melts with TiO_2 = 1–1·5 wt% at 1100–1200°C (Meen *et al.*, 1989). To circumvent problems with respect to bulk magma saturation, Green & Watson (1982) suggested that local phosphorus saturation may be responsible for tiny apatite inclusions in phenocryst feldspars from intermediate magmas. These magmas do not contain enough P_2O_5 to reach saturation levels indicated from experiments. Green & Watson (1982) therefore suggested that P_2O_5 concentrations in the melt may strongly increase near the margins of rapidly growing phenocrysts, because of slow diffusion of phosphorus away from the growing mineral. Local saturation results in precipitation of tiny apatite crystals, which become enclosed by the growing mineral. The same process could be responsible for the formation of tiny (10–50 μm) inclusions of rutile, possible monazite and apatite in cumulus garnets and pyroxenes from the pyroxenites, and may indicate that bulk melt saturation was not reached. However, apatite inclusions in the garnetites are much larger (0·2–0·5 mm) and also occur in clusters together with clinopyroxene and ilmenite, suggesting a high P_2O_5 concentration in the melt. In addition, Scharbert (1979) reported the occurrence of garnet websterites from lower Austria which contain 10 vol. % of Mg-rich ilmenite. There is no doubt that these ilmenite-rich pyroxenites reflect Ti saturation in their equilibrium melts. On the basis of these observations it seems likely that most of the parent melts were close to Ti saturation, some were Ti saturated, and in few instances (garnetites) were also P saturated. The Ti saturation condition is most easily reached by CO_2-rich magmas which may have been high-pressure precursor magmas of carbonatites, melilitites or a CO_2-rich lamprophyre-type magma. These magmas are also characterized by very high LREE abundances and hence have some important characteristics of the melts inferred to have equilibrated with the cumulus pyroxenites from lower Austria.

HFSE anomalies—source characteristic or Ti- and P-phase fractionation?

Titanium minerals also contribute to the whole-rock budget of other HFSE such as Zr and Ta. Reasonable estimates of mineral–melt partition coefficients exist for these elements even in accessory minerals such as rutile and ilmenite (Table 4). Figure 8 shows element concentration diagrams (normalized to primitive mantle values) calculated for melts in equilibrium with an MgO-rich garnet clinopyroxenite (DW321B) and an apatite–ilmenite garnetite (WV1). The garnet clinopyroxenite is representative of other samples with tiny inclusions of rutile and monazite(?). As the weight fractions of these inclusions cannot be quantified, they were not considered for equilibrium melt calculations. The influence on Ti of a few tiny grains of rutile is probably not significant, because garnet and pyroxenes contain enough Ti (0·10–0·25 wt% TiO_2) to account for the bulk-rock Ti abundance (0·2 wt% TiO_2). The negative Ti anomaly of the melt persists regardless of whether it is assumed that the melt was close to Ti saturation (carbonatite melt) or not. Rutile also affects Ta abundances. Tantalum is depleted relative to La (Fig. 8a), even though rutile is not taken into account in these calculations. Considering the compatible behaviour of Ta in rutile (Green & Pearson, 1987), these melts must have been even more depleted in Ta than is apparent from Fig. 8a. The depletion of Ti and Ta relative to the LREE in the melt can be a result of previous Ti-phase fractionation, or due to residual Ti phases in the source, or it may be an inherited feature of the source of the magma.

The equilibrium melt composition of the garnetite (Fig. 8b) was calculated assuming P and Ti saturation in a carbonatitic melt, owing to the presence of the minor phases apatite and ilmenite. Keeping the assumption of P saturation, the positive P spike never disappears even if it is assumed that

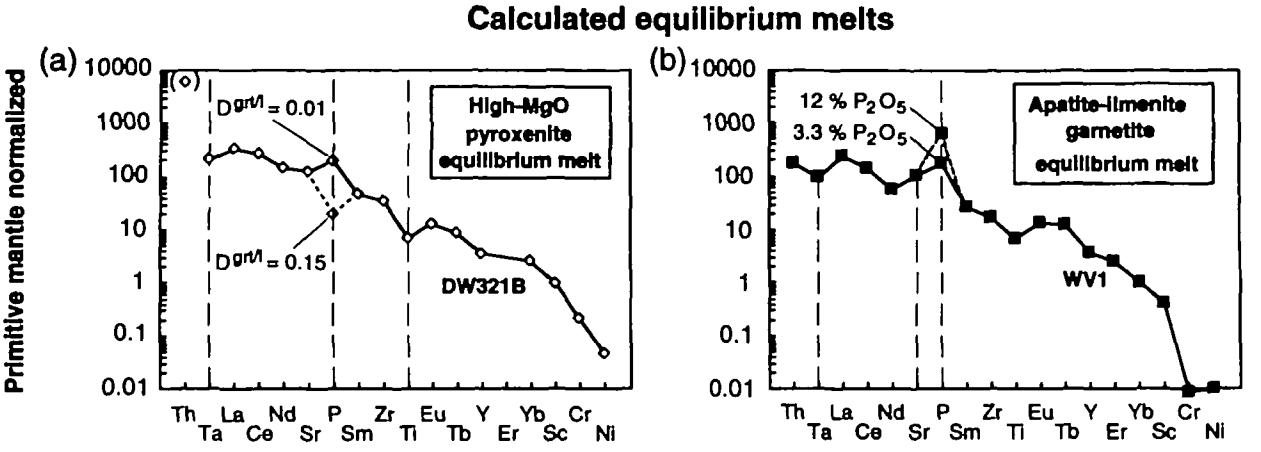

Fig. 8. Normalized element concentration diagrams of melts in equilibrium with garnet clinopyroxenite DW321B (a) and garnetite sample WV1 (b). In (a) Th is probably too high (parentheses), presumably owing to the presence of trace amounts of monazite(?) in sample DW321B. Ti saturation in a carbonatitic melt was assumed (1·2 wt% TiO_2 at 1180°C; Baker & Wyllie, 1992) based on the presence of trace amounts of rutile, which results in a weak negative Ti anomaly. P concentration in the melt depends on the choice of the garnet–melt partitioning coefficient [$D^{grt/l} = 0{\cdot}01$ for carbonatite (Baker & Wyllie, 1992); $D^{grt/l} = 0{\cdot}15$ for basalt (Thompson, 1975)]. In (b) P and Ti saturation was assumed based on the presence of apatite and ilmenite as minor phases. P shows a positive anomaly irrespective of whether a carbonatitic liquid (12% P_2O_5 solubility at 1100–1200°C; Baker & Wyllie, 1992) or a basaltic liquid (3 wt% P_2O_5 at 1100°C and 45 wt% SiO_2; Harrison & Watson, 1984) is assumed.

the melt was of basaltic composition (e.g. 3·3 wt% P_2O_5 at 1100°C and 45 wt% SiO_2 (Harrison & Watson, 1984). Weak negative Ta and Ti anomalies are also present. In addition, Fig. 8b shows a positive Sr anomaly. Th in this sample is probably controlled by apatite. Some key trace element ratios as well as Cr and Ni contents of calculated equilibrium melts from selected pyroxenites and megacrysts are given in Table 5. The high Cr but relatively low Ni contents of calculated melts in equilibrium with samples which were located close to harzburgite wallrocks (e.g. websterites and pyroxene megacrysts DW339D, DW317A, DW318) are most easily explained by partial melting of the wallrock and preferred dissolution of spinel and pyroxenes from the harzburgite.

K and Rb depletion in high-pressure cumulates

If the cumulate compositions were modified by small amounts of a trapped melt, normalized abundances of K and Rb should be at least as high as those of the LREE and one would expect the presence of minor amounts of phlogopite in equilibrium with pyroxenes and garnets. In contrast, strong depletions in K and Rb relative to the LREE and Th are characteristic of most of the garnet pyroxenites (Fig. 5). The conditions of cumulate formation as inferred from geothermobarometry (1400–1100°C at 100–120 km depth) seem to rule out that trapped melt modifies the composition of such cumulates. According to available experimental evidence, amphibole is not stable at these conditions and phlogopite may be stable up to 1200°C only (Mengel & Green, 1989). Hence, during cumulate formation, K and Rb were strongly fractionated into the remaining liquid, which apparently must have separated fairly efficiently from the cumulates. Ba has similar abundances relative to Th and La or may be slightly depleted. This cannot be explained by normal mineral–melt partitioning of a clinopyroxene–garnet assemblage (Beattie, 1993*a*; Hart & Dunn, 1993). Trace amounts of retrograde amphibole, which is preferentially found near garnet, could be the main host for Ba. However, this interpretation is only viable if the fluid, which crystallized amphibole, was strongly enriched in Ba relative to Rb and K.

Eu anomalies

As shown in Fig. 4, most pyroxenites from lower Austria have significant negative Eu anomalies. In contrast, the garnet–kyanite clinopyroxenites have positive Eu anomalies and two pyroxenites have no Eu anomalies. The large amount of REE data available for mantle xenoliths and ultramafic massifs demonstrates that Eu anomalies are not generated during melting and mineral fractionation in the spinel and garnet peridotite facies of the upper mantle [see McDonough & Frey (1989) for a review]. A similar conclusion can be drawn from REE data of most oceanic basalts and island arcs

Table 5: Cr and Ni concentrations and ratios of incompatible elements of calculated melts in equilibrium with pyroxenites and megacrysts

Sample	Cr	Ni	La/Ta	$(La/Sm)_n$	$(La/Yb)_n$	$(Tb/Yb)_n$	Sr/Nd	Zr/Sm
High-MgO pyroxenites								
DW339 D	2289	172	18	17	93	1·1	21	27
DW339 C2	300	83	13	21	80	1·3	21	
DW339 B	268	61	15	23	99	1·0	19	
DW321 B	661	98	28	7	123	3·1	14	18
Low-MgO pyroxenites and garnetites								
PW221A	94	9	8	15	150	2·2	21	23
SL58	144	53	5	4	120	6·4	31	17
DW98	77	22	21	2	36	4·4	107	13
WV1	27	22	43	9	228	11·9	27	16
WV2	51	14		4	33	3·5	22	15
Megacrysts								
DW317A(Opx)	2382	267		47	906	2·1	14	46
DW318 (Cpx)	1686	199	12	20	326	4·7	19	28

Melt compositions of the pyroxenites and megacrysts calculated using partition coefficients, relevant for basaltic systems (Table 4). Partitioning coefficients in carbonatitic systems are probably similar (Brenan & Watson, 1991; Green *et al.*, 1992). Concentrations given in p.p.m.

review]. A similar conclusion can be drawn from REE data of most oceanic basalts and island arcs (Bence, 1981). Shallow igneous differentiation processes that involve feldspars normally result in negative Eu anomalies in a wide range of magma compositions. In contrast, feldspar-bearing cumulates normally show positive Eu anomalies. Negative Eu anomalies are typical for most rocks of the upper continental crust, including sediments, because these rocks or their precursors did in most cases undergo intracrustal melting and feldspar fractionation processes (Taylor & McLennan, 1985). Eu anomalies may also form as a result of strong hydrothermal alteration and low-grade metamorphism of basalts, particularly if most of the primary phases and glass have been converted to a metamorphic mineral assemblage (Sun & Nesbitt, 1978). This process cannot explain the Eu anomalies in the garnet pyroxenites because they only contain trace amounts of retrograde minerals. Therefore, the Eu anomalies of the pyroxenites must be inherited from the melts parental to the pyroxenites. Moreover, the source region of these melts must also have been characterized by negative Eu anomalies.

DISCUSSION

High-pressure cumulates and related melts

The MgO-rich pyroxenites and related pyroxene megacrysts formed from melts with extreme LREE enrichment, strong LREE fractionation, and negative Eu and HFSE anomalies, and have high Sr isotope and low Nd isotope ratios (samples DW339B,C2,D,E; DW321A,B; DW318; DW324A; DW317A). Some of these pyroxenites show high-pressure cumulus features (e.g. modal layering), and occur in peridotites which show LREE enrichment. A pyroxenite with low MgO, negative Eu anomaly and HREE depletion has a high Sm/Nd coupled with relatively low $^{143}Nd/^{144}Nd$. The high Sm/Nd does not reflect depletion in LREE, for example, owing to partial melting, but is merely a consequence of large amounts of cumulus garnet present (~50 vol. %). This relationship is indicated by the LREE-enriched nature of the clinopyroxenes. The isotopic composition of one of the apatite–ilmenite garnetite samples (WV1) indicates that the parent melts must have formed from different precursor material compared with the MgO-rich pyroxenites.

Negative Eu anomalies, strongly fractionated REE and HREE depletion suggest that these garnet-rich rocks are related to pyroxenites such as sample SL58. Minor proportions of primary apatite and ilmenite indicate P and Ti saturation in melts parental to the garnetites. The preferential presence of these minerals in garnet-rich cumulates with high FeO contents may indicate that they crystallized together with garnet near the solidus. Variable REE fractionation of the two apatite–ilmenite garnetites and their calculated melt compositions clearly point to heterogeneous melt compositions and inherited HREE depletion of some of these melts. The strong LREE and Th enrichment of the parent melts (Fig. 8b) is suggestive of a carbonatitic, or highly alkaline melt composition (melilitite, kimberlite, lamproite or minette-type magmas). Similar ilmenite-bearing garnet pyroxenites and megacrysts have been found in alnoite from Malaita (Solomon Islands, SW Pacific; Nixon & Boyd, 1979; Nixon & Neal, 1987), and in minette from the Colorado plateau province (Ehrenberg, 1982). These cumulates probably also crystallized from CO_2-rich melts migrating in the deep lithosphere.

Mantle-derived magmas other than normal arc basalts, with isotopic compositions as extreme as those shown by the high-pressure cumulates from lower Austria, include some K-rich magmas which erupt in subduction zone settings (e.g. Roman province; Hawkesworth & Vollmer, 1979). Group II kimberlites can probably be excluded, because they only occur in early Proterozoic to Archean lithosphere. Lamproitic melt compositions are also unlikely, because lamproites are suggested to form in a Ca–Al-poor, hydrous and reduced (CO_2-poor) lithospheric environment (Foley *et al.*, 1987). The Ca–Al-rich composition of most of the high-pressure cumulates does not indicate a Ca–Al-poor magma composition. The parent melts of high-pressure cumulates from lower Austria were most probably of carbonatitic, melilititic or lamprophyre-like composition. The presence of apatite [see Yaxley *et al.* (1991)] and presumably Th-rich inclusions in garnets of some pyroxenites from lower Austria, Ti saturation considerations and Ca-rich compositions of many pyroxenites are consistent with a melilitite-like or primitive carbonatitic nature of the melts. The primary cumulus assemblage of the pyroxenites (clinopyroxene ± garnet) is also consistent with liquidus to near-solidus assemblages of CO_2- and H_2O-bearing melilitites (Brey & Green, 1977) and carbonatites (Baker & Wyllie, 1992) at 3 GPa and 1200–1300°C. The major element composition of such melts may be very different from those of melilitites or carbonatites erupted at the surface, because these melts are miscible at high pressures.

Origin of continental crust-like signatures

To explain the isotopic compositions of the high-pressure cumulates by radiogenic decay in the mantle would require a long-term enrichment of Rb relative to Sr and of the LREE relative to the MREE in their source. Such a situation is possible in old lithospheric mantle where LILE-enriched asthenospheric melts can be trapped and may develop radiogenic Sr isotope ratios over time (Kramers *et al.*, 1983). The pyroxenites from lower Austria cannot have developed their high Sr isotope ratios by *in situ* radiogenic growth because they have very low Rb/Sr ratios. Also, isotopic disequilibrium across modally zoned pyroxenites indicates a short residence time in the deep lithospheric mantle. The strong depletion and short residence time of Rb in the asthenospheric mantle, which is due to previous melt extraction and its high incompatibility (Galer & O'Nions, 1985), makes it also unlikely that the high Sr isotope ratios of the pyroxenites were generated by long-term radioactive decay in the asthenosphere. High-pressure granulites from lower Austria are of calc-alkaline composition (Carswell, 1991) and have some features in common with pyroxenites enclosed in the peridotites, for example, negative Eu, Ti, Nb and Ta anomalies. However, the pyroxenites cannot have formed by partial melting of the granulites because the latter were subducted to a depth corresponding to ~1·6–1·8 GPa only, and have unsuitable major and trace element compositions to explain the formation of the pyroxenites.

The most plausible explanation for the sediment-like isotopic composition of the garnet pyroxenites from lower Austria is that their equilibrium melts were derived from sub-lithospheric mantle which contained a component of subducted continental crust. Indirect evidence for the recycling of continental material into the mantle is given by trace element and isotope systematics of island arc and oceanic island basalts (OIBs). Island arc volcanic rocks have trace element and isotopic compositions which require a small contribution from subducted sediments (e.g. White & Patchett, 1984; White & Dupre, 1986). Furthermore, it has been suggested that some OIB were derived from plumes containing material with sediment-like isotopic compositions that once was subducted into the mantle (White, 1985). The presence of a recycled component in the high-pressure cumulates is consistent with the observed LREE enrichment (bulk

rock as well as clinopyroxenes), although other variables such as degree of partial melting also have a strong influence. Depletion of a few garnet-rich samples in HREE also favours the interpretation that some of these melts were already strongly depleted in HREE. Finally, there is no obvious process which results in negative Eu anomalies during high-pressure fractionation and mantle melting at high pressures. Consequently, the anomalies shown by the pyroxenites also must be inherited features of the melts.

Among orogenic peridotite massifs, the highly radiogenic Sr and unradiogenic Nd isotopic compositions of the pyroxenites from southern Bohemia are most similar to the garnet pyroxenites from Beni Bousera and Ronda (Kornprobst *et al.*, 1990; Pearson *et al.*, 1993). However, the latter appear to be much more variable in isotopic composition, with many samples having low Sr isotope and high Nd isotope ratios. Some of the pyroxenites from Beni Bousera have $\delta^{18}O$ values up to nine. This was interpreted to be an inherited feature from subducted oceanic crust that had been hydrothermally altered. High $^{207}Pb/^{204}Pb$ and $^{208}Pb/^{204}Pb$ ratios of clinopyroxenes from the pyroxenites and negative $\delta^{13}C$ values of graphite pseudomorphs after diamond are evidence for the presence of a component of recycled sediments (Pearson *et al.*, 1993). A significant difference between the pyroxenites from lower Austria and Beni Bousera is that the latter are strongly depleted in LREE. Some clinopyroxenes in pyroxenites from Beni Bousera have extremely high Sm/Nd ratios, which was interpreted to be the result of a recent partial remelting of the layers (Loubet & Allègre, 1982; Pearson *et al.*, 1993).

Metamorphosed crustal rocks

The garnet–kyanite pyroxenites with positive Eu anomalies (sample DW98, presumably also sample DW231A) are different from the high-pressure cumulates with respect to isotopic composition (low $^{87}Sr/^{86}Sr$ ratios and positive, moderately high ε_{Nd}), major and trace element characteristics, and mineralogy (kyanite bearing). Garnet pyroxenites of similar composition were reported from the peridotite massifs near Ronda and Beni Bousera (Suen & Frey, 1987; Kornprobst *et al.*, 1990; Pearson *et al.*, 1993). Minerals from eclogites and garnet pyroxenites enclosed in peridotite massifs from the Czech part of southern Bohemia also have elevated $^{87}Sr/^{86}Sr$ (up to 0·7054 at 335 Ma) and some of them have positive Eu anomalies too (Beard *et al.*, 1992), indicating the presence of recycled components. Positive anomalies of Eu, Sr and Ba, as well as relatively high Na, Al and Ca, and low Mg contents (relative to other pyroxenites) indicate that either these pyroxenites represent metamorphosed plagioclase-rich cumulates or the pyroxenites crystallized from melts that were derived from metamorphosed plagioclase-rich cumulates. The former hypothesis is preferred because partial melting of high-pressure equivalents of plagioclase-rich cumulates would produce silicic magmas [in analogy with partial melting of eclogite; e.g. Green (1982)]. Such magmas would become Mg rich owing to reaction with surrounding peridotite, and thus would no longer retain a major element composition close to that of plagioclase-rich cumulates. Regardless of the exact origin, the coexistence of primary garnet, clinopyroxene and kyanite constrains the high-pressure equilibration of these rocks ($P > 2{\cdot}3$–$2{\cdot}5$ GPa; Carswell *et al.*, 1989). A calc-silicate marble and enclosed Ca–Fe-rich garnet pyroxenites provide additional evidence for the recycling of crustal material to a depth of $\sim$100 km (Becker & Altherr, 1992). The isotopic compositions of these rocks are sediment like, and trace element patterns of marble samples also support a sedimentary origin.

At outcrops where the kyanite-bearing pyroxenites occur, the peridotites also contain thin garnet clinopyroxenite and websterite bands. In contrast to all the other pyroxenites, the thin garnet pyroxenite bands do not show Eu anomalies. They have flat or slightly LREE-enriched REE patterns with low to moderate REE abundances, and may reflect the passage of more depleted melts (e.g. clinopyroxenes of composite pyroxenite DW236 have only 3·6 p.p.m. Nd and 48 p.p.m. Sr; Table 3). The isotopic compositions of these pyroxenites can be explained in several ways. The pyroxenites may have crystallized from low-degree melts with isotopic compositions similar to OIB ($^{87}Sr/^{86}Sr$ 0·7034–0·7037) and evolved relatively low Nd isotopic ratios over a time span of 1–1·5 b.y. It is not clear whether such melts were derived from subducted oceanic crust, or just reflect low-degree melting of the asthenospheric MORB source. It is also possible that these pyroxenites represent relics of subducted oceanic basalts that were accreted to the deep lithosphere and underwent later high-strain deformation. If such material had lost its Rb during the subduction process, it would have been able to develop appropriate isotopic compositions during its storage in the deep lithosphere. Peridotites associated with these thin pyroxenite layers have flat to LREE-depleted REE patterns. It seems that the LREE-depleted peridotites, thin pyroxenite layers without Eu anomalies and garnet–kyanite pyroxenites with positive Eu anomalies form a distinct assemblage.

These rocks have not been found in outcrops where high-pressure cumulates with sediment-like isotopic compositions and LREE-enriched peridotites occur. The MORB- to OIB-type isotopic compositions, particularly of the former plagioclase-rich cumulates, may indicate the presence of fragments of subducted oceanic crust.

CONCLUSIONS

Major and trace element compositions of garnet pyroxenites enclosed in peridotite massifs from lower Austria indicate that most of them are high-pressure cumulates which crystallized in the deep lithosphere from low-degree melts. According to the equilibration conditions of pyroxenites and peridotites, the melts were derived from sub-lithospheric sources. Ti- and P-saturation considerations, REE–HFSE fractionations and comparison with pyroxenite xenoliths and megacryst suites found in alkaline basalts suggest that the parent melts were rich in CO_2, and most likely of primitive carbonatitic, melilitic or lamprophyre-like composition. Negative Eu anomalies and continental crust-like isotopic compositions of the high-pressure cumulates indicate the presence of subducted sediments in the sub-lithospheric portion of a mantle wedge or in a deep-seated subducting slab during the late Palaeozoic. The peridotites also contain fragments of crustal rocks which originally formed at low pressure but now yield evidence of high-pressure equilibration. These rocks are interpreted as subducted rocks, accreted to lithosphere of the hangingwall plate. Thus, the chemical composition and lithological variability of the mantle rocks from lower Austria concur with geological evidence (Carswell, 1991; Becker, submitted) that the mantle fragments were derived from the hangingwall plate of a former convergent plate margin. The most likely scenario for the formation of the high-pressure cumulates is an incipient marginal basin setting where the amount of lithospheric stretching is minor. This allows the formation of only small amounts of melts by low degrees of partial melting in the sub-lithospheric mantle (McKenzie, 1989), perhaps triggered by ascending fluids or melts derived from a subducted slab at greater depth. During further post-orogenic extension, deep lithospheric pyroxenite cumulates of such low-degree melts could become preferentially remelted. Such a remelting of enriched pyroxenites could have a profound influence on the trace element and isotopic composition of post-orogenic magmas.

ACKNOWLEDGEMENTS

This work forms part of a doctoral thesis, financially supported by the Max-Planck-Gesellschaft. I thank S. Galer, A. Hofmann, R. Oberhänsli, G. Pearson, L. Reisberg, J. Stolz and M. Wilson for improving the English and for helpful suggestions on this and earlier versions of the manuscript. G. Brey donated samples WV1 and WV2. I am grateful to H. Frohna-Binder, R. Gehann, E. Griesshaber and N. Groschopf for their help during the XRF, INAA and HPLC analysis, and H. Feldmann and S. Goldstein for their help and advice on the mass spectrometer.

REFERENCES

Alibert, C., Michard, A. & Albarede, F., 1983. The transition from alkali basalts to kimberlites: isotope and trace element evidence from melilitites. *Contributions to Mineralogy and Petrology* **82**, 176–186.

Allègre, C. J. & Turcotte, D. L., 1986. Implications of a two-component marble-cake mantle. *Nature* **323**, 123–127.

Baker, M. B. & Wyllie, P. J., 1992. High-pressure apatite solubility in carbonate-rich liquids: implications for mantle metasomatism. *Geochimica et Cosmochimica Acta* **56**, 3409–3422.

Beard, B. L., Medaris, G. L., Johnson, C. M., Brueckner, H. K. & Misar, Z., 1992. Petrogenesis of Variscan high-temperature Group A eclogites from the Moldanubian Zone of the Bohemian Massif, Czechoslovakia. *Contributions to Mineralogy and Petrology* **111**, 468–483.

Beattie, P., 1993*a*. The generation of uranium series disequilibria by partial melting of spinel peridotite: constraints from partitioning studies. *Earth and Planetary Science Letters* **117**, 379–391.

Beattie, P., 1993*b*. Uranium–thorium disequilibria and partitioning on melting of garnet peridotite. *Nature* **363**, 63–65.

Becker, H., 1996. Geochemistry of garnet peridotite massifs from lower Austria and the composition of deep lithosphere beneath a Paleozoic convergent plate margin. *Chemical Geology* (in press).

Becker, H. & Altherr, R., 1992. Evidence from ultra-high-pressure marbles for recycling of sediments into the mantle. *Nature* **358**, 745–748.

Becker, H. & Wenzel, T., 1996. Glimmerite veins in high-pressure rocks from Lower Austria—clues for the origin of high-K magmas in orogenic belts. Sixth V. M. Goldschmidt Conference, Heidelberg. *Journal of Conference Abstracts* **1**(1), 53.

Bence, A. E., 1981. Basalts as probes of planetary interiors: constraints on the chemistry and mineralogy of their source regions. In: Basaltic Volcanism Study Project (ed.) *Basaltic Volcanism on the Terrestrial Planets*. Oxford: Pergamon Press, pp. 311–339.

Benjamin, T., Heuser, W. R., Burnett, D. S. & Seitz, M. G., 1980. Actinide crystal–liquid partitioning for clinopyroxene and $Ca_3(PO_4)_2$. *Geochimica et Cosmochimica Acta* **44**, 1251–1264.

Brenan, J. M. & Watson, E. B., 1991. Partitioning of trace elements between carbonate melt and clinopyroxene and olivine at mantle P–T conditions. *Geochimica et Cosmochimica Acta* **55**, 2203–2214.

Brey, G. & Green, D. H., 1977. Systematic study of liquidus phase relations in olivine melilitite + H_2O + CO_2 at high pressures and petrogenesis of olivine melilitite magma. *Contributions to Mineralogy and Petrology* **61**, 141–162.

Carswell, D. A., 1991. Variscan high P–T metamorphism and uplift history in the Moldanubian Zone of the Bohemian Massif in lower Austria. *European Journal of Mineralogy* **3**, 323–342.

Carswell, D. A., Möller, C. & O'Brien, P. J., 1989. Origin of sapphirine–plagioclase symplectites in metabasites from Mitterbachgraben, Dunkelsteiner Wald granulite complex, lower Austria. *European Journal of Mineralogy* **1**, 455–466.

Cassidy, R. M., 1988. Determination of rare-earth elements in rocks by liquid chromatography. *Chemical Geology* **67**, 185–195.

Conquere, F., 1977*a*. Pétrologie des pyroxénites litées dans les complexes de l'Ariège et autres gisements de lherzolites à spinelle. Compositions minéralogiques et chimiques, évolution des conditions d'équilibre des pyroxénites. *Bulletin de la Société Français de Minéralogie et Cristallographie* **100**, 42–80.

Conquere, F., 1977*b*. Pétrologie des pyroxénites litées dans les complexes de l'Ariège et autres gisements de lherzolites à spinelle. Pétrogenèse. *Bulletin de la Société Française de Minéralogie et Cristallographie* **100**, 123–137.

Dallmeyer, R. D., Neubauer, F. & Höck, V., 1992. Chronology of late Paleozoic tectonothermal activity in the southeastern Bohemian massif, Austria (Moldanubian and Moravo-Silesian zones): $^{40}Ar/^{39}Ar$ mineral age controls. *Tectonophysics* **210**, 135–153.

Davies, G. R., Gledhill, A. & Hawkesworth, C., 1985. Upper crustal recycling in southern Britain: evidence from Nd and Sr isotopes. *Chemical Geology* **75**, 1–12.

Edwards, C. M. H., Morris, J. D. & Thirlwall, M. F., 1993. Separating mantle from slab signatures in arc lavas using B/Be and radiogenic isotope systematics. *Nature* **362**, 530–533.

Ehrenberg, S. N., 1982. Rare earth element geochemistry of garnet lherzolite and megacrystalline nodules from minette of the Colorado Plateau province. *Earth and Planetary Science Letters* **57**, 191–210.

Evensen, N. M., Hamilton, P. J. & O'Nions, R. K., 1978. Rare-earth abundances in chondritic meteorites. *Geochimica et Cosmochimica Acta* **42**, 1199–1212.

Foley, S. F., Venturelli, G., Green, D. H. & Toscani, L., 1987. The ultrapotassic rocks: characteristics, classification, and constraints for petrogenetic models. *Earth-Science Reviews* **24**, 81–134.

Galer, S. J. G. & O'Nions, R. K., 1985. Residence times of thorium, uranium and lead in the mantle with implications for mantle convection. *Nature* **316**, 778–782.

Green, D. H. & Ringwood, A. E., 1967. The genesis of basaltic magmas. *Contributions to Mineralogy and Petrology* **15**, 103–190.

Green, T. H., 1982. Anatexis of mafic crust and high pressure crystallization of andesite. In: Thorpe, R. S. (ed.) *Andesites*. New York: Wiley, pp. 466–487.

Green, T. H. & Pearson, N. J., 1986. Ti-rich accessory phase saturation in hydrous mafic–felsic compositions at high *P,T*. *Chemical Geology* **54**, 185–201.

Green, T. H. & Pearson, N. J., 1987. An experimental study of Nb and Ta partitioning between Ti-rich minerals and silicate liquids at high pressure and temperature. *Geochimica et Cosmochimica Acta* **51**, 55–62.

Green, T. H. & Watson, E. B., 1982. Crystallization of apatite in natural magmas under high pressure, hydrous conditions, with particular reference to 'orogenic' rock series. *Contributions to Mineralogy and Petrology* **79**, 96–105.

Green, T. H., Adam, J. & Sie, S. H., 1992. Trace element partitioning between silicate minerals and carbonatite at 25 kbar and application to mantle metasomatism. *Mineralogy and Petrology* **46**, 179–184.

Harrison, T. M. & Watson, E. B., 1984. The behaviour of apatite during crustal anatexis: equilibrium and kinetic considerations. *Geochimica et Cosmochimica Acta* **48**, 1467–1477.

Hart, S. R. & Dunn, T., 1993. Experimental cpx/melt partitioning of 24 trace elements. *Contributions to Mineralogy and Petrology* **113**, 1–8.

Hauri, E. H., Shimizu, N., Dieu, J. J. & Hart, S. R., 1993. Evidence for hotspot-related carbonatite metasomatism in the oceanic upper mantle. *Nature* **365**, 221–227.

Hawkesworth, C. J. & Vollmer, R., 1979. Crustal contamination versus enriched mantle: $^{143}Nd/^{144}Nd$ and $^{87}Sr/^{86}Sr$ evidence from Italian volcanics. *Contributions to Mineralogy and Petrology* **69**, 151–165.

Hearn, B. C., 1989. Alkalic ultramafic magmas in north–central Montana, USA: genetic connections of alnöite, kimberlite, and carbonatite. In: Jaques, A. L., Ferguson, J. & Green, D. H. (eds) *Kimberlites and Related Rocks I: their Composition, Occurrence, Origin and Emplacement*. Melbourne, Vic.: Blackwell, pp. 109–119.

Hofmann, A. W., 1988. Chemical differentiation of the Earth: the relationship between mantle, continental crust and oceanic crust. *Earth and Planetary Science Letters* **90**, 297–314.

Irving, A. J., 1978. A review of experimental studies of crystal/liquid trace element partitioning. *Geochimica et Cosmochimica Acta* **42**, 743–770.

Irving, A. J. & Frey, F. A., 1978. Distribution of trace elements between garnet megacrysts and host volcanic liquids of kimberlitic to rhyolitic composition. *Geochimica et Cosmochimica Acta* **42**, 771–787.

Irving, A. J. & Frey, F. A., 1984. Trace element abundances in megacrysts and their host basalts: constraints on partition coefficients and megacryst genesis. *Geochimica et Cosmochimica Acta* **48**, 1201–1221.

Jacobsen, S. B. & Wasserburg, G. J., 1980. Sm–Nd isotopic evolution of chondrites. *Earth and Planetary Science Letters* **50**, 139–155.

Johnson, K. T. M., 1993. Experimental cpx/ and garnet/melt partitioning of REE and other trace elements. *EOS* **74**, 658.

Kelemen, P. B., Shimizu, N. & Dunn, T., 1993. Relative depletion of niobium in some arc magmas and the continental crust: partitioning of K, Nb, La and Ce during melt/rock reaction in the upper mantle. *Earth and Planetary Science Letters* **120**, 111–134.

Kornprobst, J., 1969. Le massif ultrabasique des Beni Bouchera (Rif Interne, Maroc): étude des peridotites de haute temperature et de haute pression, et des pyroxénolites, à grenat ou sans grenat, qui leur sont associées. *Contributions to Mineralogy and Petrology* **23**, 283–322.

Kornprobst, J., Piboule, M., Roden, M. & Tabit, A., 1990. Corundum-bearing garnet clinopyroxenites at Beni Bousera (Morocco): original plagioclase-rich gabbros recrystallized at depth within the mantle? *Journal of Petrology* **31**, 717–745.

Kosler, J., Aftalion, M. & Bowes, D. R., 1993. Mid–late Devonian plutonic activity in the Bohemian massif: U–Pb zircon isotopic evidence from the Staré Sedlo and Mirotice gneiss complexes, Czech Republic. *Neues Jahrbuch für Mineralogie, Monatshefte* 417–431.

Kramar, U. & Puchelt, H., 1982. Reproducibility tests for INAA determinations with AGV-1, BCR-1 and GSP-1 and new data for 17 geochemical reference materials. *Geostandards Newsletter* **6**, 221–227.

Kramers, J. D., Roddick, J. C. M. & Dawson, J. B., 1983. Trace element and isotope studies on veined, metasomatic and 'MARID' xenoliths from Bultfontein, South Africa. *Earth and Planetary Science Letters* **65**, 90–106.

Liew, T. C. & Hofmann, A. W., 1988. Precambrian crustal components, plutonic associations, plate environment of the

Hercynian Fold Belt of central Europe: indications from a Nd and Sr isotopic study. *Contribution to Mineralogy and Petrology*, **98**, 129–138.

Loubet, M. & Allègre, C. J., 1982. Trace elements in orogenic lherzolites reveal the complex history of the upper mantle. *Nature* **298**, 809–814.

Matte, P., Maluski, H., Rajlich, P. & Franke, W., 1990. Terrane boundaries in the Bohemian massif: result of large-scale Variscan shearing. *Tectonophysics* **177**, 151–170.

McCallum, I. S. & Charette, M. P., 1978. Zr and Nb partitioning coefficients: implications for the genesis of Mare basalts, KREEP, and sea floor basalts. *Geochimica et Cosmochimica Acta* **42**, 859–869.

McDonough, W. F. & Frey, F. A., 1989. Rare earth elements in upper mantle rocks. In: Lipin, B. R. & McKay, G. A. (eds) *Geochemistry and Mineralogy of Rare Earth Elements*. Washington, DC: Mineralogical Society of America, pp. 99–145.

McDonough, W. F., Sun, S.-S., Ringwood, A. E., Jagoutz, E. & Hofmann, A. W., 1992. Potassium, rubidium, and cesium in the Earth and Moon and the evolution of the mantle of the Earth. *Geochimica et Cosmochimica Acta* **56**, 1001–1012.

McKenzie, D., 1989. Some remarks on the movement of small melt fractions in the mantle. *Earth and Planetary Science Letters* **95**, 53–72.

Meen, J. K., Ayers, J. C. & Fregeau, E. J., 1989. A model of mantle metasomatism by carbonated alkaline melts: trace element and isotopic compositions of mantle source regions of carbonatite and other continental igneous rocks. In: Bell, K. (ed.) *Carbonatites—Genesis and Evolution*. London: Unwin Hyman, pp. 464–499.

Mengel, K., & Green, D. H., 1989. Stability of amphibole and phlogopite in metasomatized peridotite under water-saturated and water-undersaturated conditions. In: *Kimberlites and Related Rocks. Vol. I. Their Composition, Occurrence, Origin and Emplacement. Special Publication, Geological Society of Australia* **14**, 571–581.

Nelson, D. R., Shivas, A. R., Chappell, B. W. & McCulloch, M. T., 1988. Geochemical and isotopic systematics in carbonatites and implications for the evolution of ocean-island sources. *Geochimica et Cosmochimica Acta* **52**, 1–17.

Nixon, P. H. & Boyd, F. R., 1979. Garnet bearing lherzolites and discrete nodule suites from the Malaita alnoite, Solomon islands, S.W. Pacific, and their bearing on oceanic mantle composition and geotherm. In: Boyd, F. R. & Meyer, H. O. A. (eds) *The Mantle Sample: Inclusions in Kimberlites and Other Volcanics*. Washington, DC: American Geophysical Union, pp. 400–423.

Nixon, P. H. & Neal, C. R., 1987. Ontong Java Plateau: deep-seated xenoliths from thick oceanic lithosphere. In: Nixon, P. H. (ed.) *Mantle Xenoliths*. New York: John Wiley, pp. 335–345.

O'Reilly, S. Y., Griffin, W. L. & Ryan, C. G., 1991. Residence of trace elements in metasomatized spinel lherzolite xenoliths: a proton-microprobe study. *Contributions to Mineralogy and Petrology* **109**, 98–113.

Pallister, J. S. & Knight, R. J., 1981. Rare-earth element geochemistry of the Samail Ophiolite near Ibra, Oman. *Journal of Geophysical Research* **86**, 2673–2697.

Pearson, D. G., Davies, G. R., Nixon, P. H., Greenwood, P. B. & Mattey, D. P., 1991. Oxygen isotope evidence for the origin of pyroxenites in the Beni Bousera peridotite massif, North Morocco: derivation from subducted oceanic lithosphere. *Earth and Planetary Science Letters* **102**, 289–301.

Pearson, D. G., Davies, G. R. & Nixon, P. H., 1993. Geochemical constraints on the petrogenesis of diamond facies pyroxenites from the Beni Bousera peridotite massif, north Morocco. *Journal of Petrology* **34**, 125–172.

Polvé, M. & Allègre, C. J., 1980. Orogenic lherzolite complexes studied by ^{87}Rb–^{87}Sr: a clue to understand the mantle convection process. *Earth and Planetary Science Letters* **51**, 71–93.

Porcelli, D. R., O'Nions, R. K., Galer, S. J. G., Cohen, A. S. & Mattey, D. P., 1992. Isotopic relationships of volatile and lithophile trace elements in continental ultramafic xenoliths. *Contributions to Mineralogy and Petrology* **110**, 528–538.

Puchelt, H. & Kramar, U., 1981. New analytical data and homogeneity of BHVO-1. *Geostandards Newsletter* **5**, 87–94.

Rudnick, R. L., McDonough, W. F. & Chappell, B. W., 1993. Carbonatite metasomatism in the northern Tanzanian mantle: petrographic and geochemical characteristics. *Earth and Planetary Science Letters* **114**, 463–475.

Ryerson, F. J. & Watson, E. B., 1987. Rutile saturation in magmas: implications for Ti–Nb–Ta depletion in island-arc basalts. *Earth and Planetary Science Letters* **86**, 225–239.

Scharbert, H. G., 1979. Mg-reicher Ilmenit in einem Granatwebsterit im Granulitkörper von St. Leonhard, Mittleres Kamptal, Niederösterreich. *Anzeiger der Österreichischen Akademie der Wissenschaften, Mathematisch-Naturwissenschaftliche Klasse* **1979**, 161–165.

Scharbert, H. G. & Carswell, D. A. 1983. Petrology of garnet–clinopyroxene rocks in a granulite facies environment, Bohemian massif of Lower Austria. *Bulletin de Minéralogie* **106**, 761–779.

Shimizu, N. & Kushiro, I., 1975. The partitioning of rare earth elements between garnet and liquid at high pressures: preliminary experiments. *Geophysical Research Letters* **2**, 413–416.

Smewing, J. D., 1981. Mixing characteristics and compositional differences in mantle-derived melts beneath spreading axes: evidence from cyclically layered rocks in the ophiolite of north Oman. *Journal of Geophysical Research* **86**, 2645–2659.

Stosch, H.-G. & Lugmair, G. W., 1984. Evolution of the lower continental crust: granulite facies xenoliths from the Eifel, West Germany. *Nature* **311**, 368–370.

Suen, C. J. & Frey, F. A., 1987. Origins of the mafic and ultramafic rocks in the Ronda peridotite. *Earth and Planetary Science Letters* **85**, 183–202.

Sun, S. S. & McDonough, W. F., 1989. Chemical and isotopic systematics of oceanic basalts: implications for mantle composition and processes. In: Saunders, A. D. & Norry, M. J. (eds) *Magmatism in Ocean Basins*. London: Geological Society of London, pp. 313–345.

Sun, S.-S. & Nesbitt, R. W., 1978. Petrogenesis of Archean ultrabasic and basic volcanics: evidence from rare earth elements. *Contributions to Mineralogy and Petrology* **65**, 301–325.

Tatsumoto, M., Basu, A. R., Wankang, H., Junwem, W. & Guanghong, X., 1992. Sr, Nd and Pb isotopes of ultramafic xenoliths in volcanic rocks of Eastern China: enriched components EM I and EM II in subcontinental lithosphere. *Earth and Planetary Science Letters* **113**, 107–128.

Taylor, S. R. & McLennan, S. M., 1985. *The Continental Crust: its Composition and Evolution*. Oxford: Blackwell.

Thompson, R. N., 1975. Is upper-mantle phosphorus contained in sodic garnet? *Earth and Planetary Science Letters* **26**, 417–424.

Voshage, H., Sinigoi, S., Mazzucchelli, M., Demarchi, G., Rivalenti, G. & Hofmann, A. W., 1988. Isotopic constraints on the origin of ultramafic and mafic dikes in the Balmuccia peridotite (Ivrea Zone). *Contributions to Mineralogy and Petrology* **100**, 261–267.

Wallace, M. E. & Green, D. H., 1988. An experimental determination of primary carbonatite magma composition. *Nature* **335**, 343–346.

Watson, E. B. & Green, T. H., 1981. Apatite/liquid partition coefficients for the rare earth elements and strontium. *Earth and Planetary Science Letters* **56**, 405–421.

Wendlandt, R. F., 1990. Partitioning of niobium and tantalum between rutile and silicate melt. *EOS* **71**, 1658.

Wendt, J. I., Kröner, A., Todt, W. & Fiala, J., 1994. U–Pb–zircon and Sm–Nd dating of Moldanubian high-*P*, high-*T* granulites from south Bohemia. *Journal of the Geological Society, London* **151**, 83–90.

White, W. M., 1985. Sources of oceanic basalts: radiogenic isotope evidence. *Geology* **13**, 115–118.

White, W. M. & Dupre, B., 1986. Sediment subduction and magma genesis in the Lesser Antilles: isotopic and trace element constraints. *Journal of Geophysical Research* **91**, 5927–5941.

White, W. M. & Patchett, P. J., 1984. Hf–Nd–Sr isotopes and incompatible element abundances in island arcs: implications for magma origins and crust–mantle evolution. *Earth and Planetary Science Letters* **67**, 167–185.

Yaxley, G. M., Crawford, A. J. & Green, D. H., 1991. Evidence for carbonatite metasomatism in spinel peridotite xenoliths from western Victoria, Australia. *Earth and Planetary Science Letters* **107**, 305–317.

RECEIVED AUGUST 14, 1995
REVISED TYPESCRIPT ACCEPTED FEBRUARY 26, 1996

APPENDIX

Analytical techniques

Bulk-rock X-ray fluorescence (XRF) analyses were carried out at Institut für Petrographie und Geochemie, Universität Karlsruhe and at Mineralogisches Institut, Universität Mainz. Major elements were determined on pellets made by fusion of a Li-borate flux–sample mixture. Reproducibilities of major elements are better than 2%, except P and Mn, which are better than 15%. Trace elements (Ba, Cr, Ni, Ga, Nb, Rb, Sr, Zr, Zn and Y) were determined on pressed powder pellets. Reproducibilities estimated from basic and ultrabasic reference samples are better than 5% for Zr, Zn, Y, Sr and Ni, better than 10% for Cr, and better than 20% for Rb. Although Ba abundances sometimes are close to detection limit (30 p.p.m.), the agreement with INAA results is within 10–30%. Total carbon contents were determined on a IR-based Carbon-Sulfur Analyser (CSA302, Leybold-Heräus) at Karlsruhe. INAA was used to determine Na_2O, Fe_2O_{3tot}, Sc, Co, Cs, La, Ce, Sm, Eu, Tb, Yb, Lu, Hf, Ta and Th (in some samples also Cr, Ni, Zn, Rb, Ba, Nd, Gd, Ho, Tm and U). Procedures at Karlsruhe were outlined by Puchelt & Kramar (1981) and Kramar & Puchelt (1982). Samples (~200 mg), reference samples AGV-1 and BHVO-1, and standard solutions were irradiated for 5 h in a TRIGA reactor at Krebsforschungszentrum Heidelberg at a neutron flux of 8×10^{12} neutrons cm^{-2} s^{-1}. Gamma spectra were measured using GeLi (150–2000 keV) and high-purity Ge (30–210 keV) detectors. Reproducibilities of Na, Fe, Sc, Cr, Co, La, Sm, Ta and Th are 2% or better. Reproducibilities of Eu, Tb, Hf are 2–5%, those of Ce, Zn, Tm and Yb 5–10%, and those of Nd, Ni, Cs, Ba, Gd, Lu and U 10–30%.

The HPLC technique (Cassidy, 1988) has been chosen as an additional method to measure REE, particularly to check the quality of INAA analyses of some pyroxenites. Reproducibilities in the concentration range of the pyroxenites are 5–10% or better. Figure A1 shows a comparison of HPLC, INAA and isotope dilution (ID) (Nd and Sm only) REE data for pyroxenite and megacryst samples. Agreement for most REE is better than 10%.

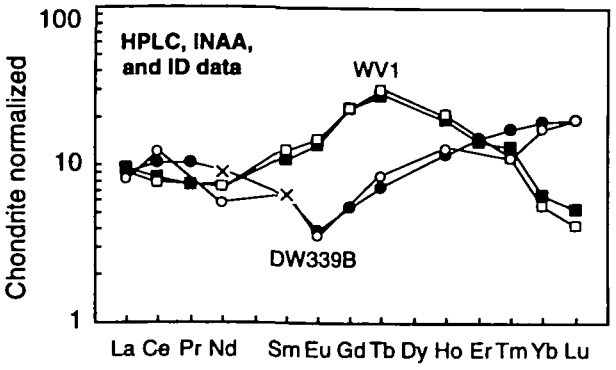

Fig. A1. Comparison of results from HPLC (filled symbols), INAA (open symbols) and ID (Nd and Sm, crosses) for garnet-rich pyroxenite DW339B and garnet megacryst sample WV1.

Sr and Nd isotope compositions and Nd, Sm, Sr and Rb concentrations of minerals and some bulk rocks were measured using ID–thermal ionization mass spectrometry (ID–TIMS) techniques. Minerals were separated with a magnetic separator, washed in an ultrasonic bath, and hand-picked under a microscope to a high degree of purity. Coarse grain size fractions were crushed in an agate mortar under alcohol. Clinopyroxenes and garnets were leached first in 6 N HNO_3 for 1 h, washed in an ultrasonic bath for 5 min, and then repeatedly rinsed with ultrapure water. The same procedure was repeated several times with 3 N HCl. Except for one sample (DW317A), whole rocks were not leached, as Nd isotopic compositions and Sm and Nd concentrations were obtained on the same sample. Amphiboles were washed in 2·5 M HCl and phlogopite was washed in cold 0·1 M HCl for a few minutes. After spiking with mixed ^{149}Sm–^{150}Nd and ^{85}Rb–^{84}Sr spikes, the samples were dissolved in screw-top Teflon beakers. Owing to the very low Rb and Sr concentrations of the garnets, aliquots of the sample were spiked after dissolution so as to measure concentrations and isotopic composition separately. Details of the separation of Rb, Sr, Sm and Nd have been given by White & Patchett (1984). Blanks in 1993 for clinopyroxene and garnet chemistry were <50 pg for Nd and Sm (<8–30 pg 1991–1992) and <130 pg and <30 pg for Sr and Rb (<38–94 pg and <21 pg 1991–1992). The $^{87}Sr/^{86}Sr$ ratio of the blank was 0·716 ± 2. For garnets with very low Sr concentrations a blank correction was applied on the $^{87}Sr/^{86}Sr$ ratio. Isotopic ratios were measured on two Finnegan MAT 261 mass spectrometers with multiple collectors operating in the static (Nd, Sm, Sr) and dynamic (Sr, Rb) mode. Errors on isotope ratios are always given as the last digits of the ratio and are $2\sigma_m$ in-run errors (samples) and 2σ errors (standards). Frequent measurements of the La Jolla Nd standard at intensities similar to sample runs yielded $^{143}Nd/^{144}Nd = 0{\cdot}511838 \pm 25$ (2σ, MS 1, $n = 44$, fractionation corrected to $^{146}Nd/^{144}Nd = 0{\cdot}7129$) and $^{143}Nd/^{144}Nd = 0{\cdot}511856 \pm 24$ (2σ, MS 2, $n = 4$). All $^{143}Nd/^{144}Nd$ ratios are corrected to a value of 0·511858 for the La Jolla Nd standard. $^{147}Sm/^{144}Nd$ ratios were measured to a precision of 0·1–0·3%. Reproducibilities of the Sr standard (NBS 987) are: $^{87}Sr/^{86}Sr = 0{\cdot}710228 \pm 24$ (2σ, dynamic on MS 1, $n = 18$), $^{87}Sr/^{86}Sr = 0{\cdot}710242 \pm 34$ (2σ, static on MS 1,

$n = 20$) and $^{87}Sr/^{86}Sr = 0{\cdot}710225 \pm 21$ (2σ, static on MS 2, $n = 6$). Fractionation was corrected to $^{86}Sr/^{88}Sr = 0{\cdot}1194$. All $^{87}Sr/^{86}Sr$ ratios of samples are given relative to a $^{87}Sr/^{86}Sr$ ratio of 0·710230 for the NBS 987 standard. Rb was measured dynamically by SEM. External reproducibilities of $^{87}Rb/^{86}Sr$ ratios are not better than 1·5–2%. ε_{Nd} values were calculated using $^{143}Nd/^{144}Nd = 0{\cdot}512638$ and $^{147}Sm/^{144}Nd = 0{\cdot}1966$ for the present-day bulk silicate Earth (Jacobsen & Wasserburg, 1980).